

A kinetic model to simulate charge flow through an electrochemical half cell

Diego Veloza-Diaz,¹ Friederike Schmid,¹ Robinson Cortes-Huerta^{**},² Pietro Ballone,² and Nancy C. Forero-Martinez^{*1}

¹*Institut für Physik, Johannes Gutenberg-Universität Mainz,*

Staudingerweg 9, 55128 Mainz, Germany

²*Max Planck Institute for Polymer Research,*

Ackermannweg 10, 55128, Mainz, Germany

Abstract

A kinetic model of the electron transfer at the electrode / electrolyte solution interface is developed, implemented in a Monte Carlo framework, and applied to simulate this process in idealised systems consisting of the primitive model of electrolyte solutions limited by an impenetrable conducting surface. In the present implementation, a charged, spherical interface surrounding an equally spherical sample of electrolyte solution is introduced to model a single-electrode system, providing the computational analog to the conceptual half-cell picture that is widely used in electrochemistry. The electron transfer itself is described as a simple surface hopping process underlying a first order reaction corresponding to one of the coupled M/M^+ and X^-/X half reactions. Then, the electron transfer at the interface is combined with the self-diffusion of ions in the electrolyte solutions whose role is to supply reagents and disperse products, allowing the system to settle in a stationary non-equilibrium state. Simulations for the primitive model of electrolyte in contact with a charged impenetrable surface show that, after a brief transient, the samples sustain a steady current through the electrolyte solution. The results quantify the dependence of the current on: the overall charge of the electrode, the electrolyte concentration, the solvent viscosity and the kinetic parameter k_e that represents the rate of the electron transfer for each ion in contact with the electrode. Since the simulated interface is very idealised, strategies to overcome the limitations of the present model are outlined and briefly discussed.

* **Corresponding author:** nforerom@uni-mainz.de

** **Corresponding author:** corteshu@mpip-mainz.mpg.de

I. INTRODUCTION

The transfer of electrons across the interface between a metal electrode and an electrolyte solution is a complex and fascinating phenomenon of great conceptual and practical interest, which underlies the functioning of both batteries and electrochemical cells, and plays a role in a variety of other topics, from catalysis to corrosion.¹ For this reason, a sizeable portion of electrochemistry is devoted to this phenomenon,² whose full understanding, however, is still elusive.

The feeling of incompleteness concerns especially the theoretical and computational description, since the electron transfer at the electrode / electrolyte interface encompasses a broad range of aspects, whose analysis requires approaches that are difficult to combine into a single scheme. Exemplary in this respect are the joint quantum / classical mechanics aspect of the electron transfer between electrode and ions in solution, the interplay of statistical mechanics and electronic structure methods that are both essential for a full description of the interface and of its electrification, and the important role of steady state non-equilibrium conditions that characterise the normal operation of every electrochemical device.

For the sake of definiteness, in what follows the attention will be focused on the electrochemical cell case, in which the flow of electrons forced, for instance, by a battery drives a chemical reaction. The model discussed in the following sections, in particular, aims at reproducing the behaviour of one half of the device, in which electrons exiting the cathode reduce ($M^+ + e \rightarrow M$) the cations in solution. This mode of operation assumes that the energy of the electronic states on the metal electrode and ions in solution reflects the distribution schematically given in Fig. 1. Extending the model to the oxidation taking place at the anion is trivial, and the two half-reactions can be combined to model either an electrochemical or a Voltaic cell.

A crucial portion of the whole problem concerns the inner interfacial region (which could be identified with the Helmholtz layer³), encompassing a thin layer on both sides of the geometric interface. In this region, ions change their oxidation state, while shedding or greatly reorganising their hydration shell, a process associated with a free energy barrier which is known as *reorganisation energy*.⁴⁻⁶ This has to take place while the transferred electron adapts to the qualitatively different condition on the two sides of the interface, consisting of localised orbitals and sharp energy eigenvalues on the electrolyte side, versus delocalised orbitals and energy bands on the metal side. The combination of these effects, i.e., the reorganisation energy and

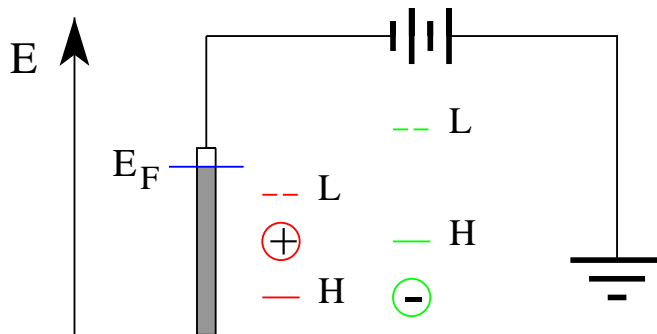


FIG. 1: Schematic diagram of the half-cell model. The electron energy is measured on the common scale indicated by the vertical axis on the left. The atomic-like energy levels on the ions are indicated by a continuous (HOMO: highest occupied molecular orbital) and dashed (LUMO: lowest unoccupied molecular orbital) segment, respectively.

the electronic transition, determine the electron transfer rate k_e whose computation is possibly the most challenging part of the entire problem.⁷ Also important, however, is to understand how the electronic processes at the interface couple to the current that has to flow in the electrolyte solution to keep the system in a steady state. Crucial, in this respect, is understanding the influence of the interface electrification, represented primarily by the interfacial double layer, on the electron transfer process and on its coupling with the current flowing through the electrolyte. Covering all these different aspects presents the additional challenge of matching phenomena developing over different size and time scales.

Ideally, one would like to have a unique framework suitable to follow the time evolution of an electrochemical cell, joining all the different aspects that it encompasses. In perspective, there is the feeling that ab-initio approaches, and ab-initio simulation methods in particular,⁸ hold the promise to fulfill this role. However, both the cost and the conceptual limitations of current methods that involve density functional theory (DFT) in its computationally viable approximations, prevent ab-initio approaches to fully meet these expectations. First of all, most ab-initio / molecular dynamics simulation methods require that the time evolution of

the system is adiabatic, i.e., it takes place on a single Born-Oppenheimer potential energy surface. Hence, popular ab-initio simulation methods are devised in such a way to describe the Newtonian dynamics of atoms and ions, while electrons follow a fake dynamics whose aim is to keep them at or close to the minimum of the functional which gives the potential energy of the electron subsystem as a function of a continuous 3D distribution function that represents the electron density. As a result, it is difficult to interpret the time evolution of the electron density as given by these methods in terms of a real-time dynamics, if not in a very smeared and averaged way. In particular, ab-initio simulation approaches lose the particle-like dynamics of the electrons, that include the granularity, randomness and jump-like features that underly the time evolution of electrons in electrochemical systems. Because of these reasons, it is still desirable to develop computationally less demanding methods, even at the cost of introducing drastic simplifications.

In undertaking this task, it might be useful to summarise the aspects that the model is expected to reproduce. First, the charge transfer is a quantum mechanical process that discontinuously changes the oxidation state of the ions. The granularity of the process, arising from the multitude of discrete electron transfer events, is a crucial aspect that the model need to retain to faithfully reproduce correlations among transfer events, as well as the noise inherent in the flow of charge through the system. The electronic charge of the metal, in turn, is quickly restored by a generator of continuous electric current, such as a battery, and, to all purposes, it can be considered constant during the electrochemical device operation. The surface charge σ of the electrode is not the primary cause of the electron transfer, which is instead driven by the relative energy and spatial superposition of electron states on the metal and on the ions, see Fig. 1. The surface charge, however, is still an important parameter, as confirmed by the simulation results shown below. Moreover, its value as a function of the applied potential defines the potential of zero (surface) charge or PZC, for which σ vanishes, which is a very important reference state for the electrode.⁹

The electronic part of the charge transfer concerns ions in the immediate vicinity of the electrode, a population that in the following will be labelled as *active*. In most cases the charge transfer has to overcome a free energy barrier. Hence, this process is slow on the typical time scale of other microscopic processes taking place in the system. Defining the rates k_e as the average number of events *per active ion* and per unit of time, the expected values are somewhat less than one event per active ion per nanosecond. Despite being slow, the charge transfer

would eventually deplete the inner layer populated by ions in close contact with the electrode, unless another mechanism, i.e., self-diffusion, to some extent compensates the charge transfer, tending to regenerate the equilibrium distribution of ions in the system. The compensation, however, is not complete. At the conditions of the simulations presented below, the alteration of the charge density profile in the vicinity of the electrode due to electron transfer, although fairly small, is apparent and can be accurately computed. It is important to remark that, at the same conditions, the ionic diffusion in the electrolyte solution runs on a faster time scale than the electron transfer process. Detailed atomistic simulations¹⁰ show that the velocity autocorrelation function for simple electrolyte ions decays exponentially with a time constant of about 1 ps. This is therefore the time needed to a diffusing ion to lose memory of its direction, making its trajectory practically and conceptually similar to a Brownian random walk. It is important to remark that this (ps) time scale is orders of magnitude faster than the electron transfer time scale given by the inverse of k_e .

The crucial problem in developing the model consists in synchronising the two essential aspects, i.e., the charge transfer⁷ and the ionic diffusion and electrical conductivity on the electrolyte side,¹¹ mixing them in the correct way that reflects the faster time scale of diffusion with respect to the kinetics of the single electron transfer. To this aim, we will resort to concepts inspired by the well known kinetic Monte Carlo algorithm,^{12,13} but also sharing aspects, algorithms and limitations with standard methods to simulate chemical kinetics. Their combination aims at covering long time intervals, retaining sufficient temporal and spatial resolution to faithfully reproduce the mutual effects of the two dominant processes.

As a side issue, a new geometric representation of electrode / electrolyte interfaces has been introduced, motivated by the following considerations. Electrochemical cells and batteries always involve two interfaces of opposite polarity. In real, macroscopic systems, the two sides of an electrochemical cell are both in equilibrium with a common neutral bulk electrolyte solution. This has motivated the usage in electrochemistry of the half cell (or half battery) concept. We attempt to develop a similar conceptual tool, introducing a spherical electrode which, combined with the grand canonical Monte Carlo (GCMC) simulation method is meant to represent a single one of the two sides of any electrochemical cell. As it is often the case, this model has both advantages and a few disadvantages with respect to the planar slab model of the electrochemical cell, as will be briefly discussed in the paper. Nevertheless, the new electrode geometry is an additional element in the computational toolkit available for electrochemical studies, and in

the present study, it allows us to focus on the narrow interfacial region, excluding any possible interference with the other side of the cell, despite the still microscopic/mesoscopic size of the simulation cell.

II. MODEL AND METHOD

For the sake of clarity and simplicity, the computational approach is presented and tested for a very idealised model of metal/electrolyte interface, similar to those used in early stages of computer simulation,¹⁴ but many of the details and realism of current atomistic force-field models can easily be reintroduced at a later stage.

The electrolyte-water solution is represented by the primitive model,¹⁵ which is an implicit solvent model, consisting of an assembly of N charged hard spheres. In other terms, the water solvent enters the model only as the dielectric medium that decreases the Coulomb interaction among ions by a factor equal to the static dielectric constant $\epsilon_0 = 78.5$. The ion-ion interaction is of the hard-sphere type, supplemented by Coulomb charges at the centre of each sphere. In general, the choice of the hard sphere diameters, i.e., d_{++} , d_{+-} , d_{--} for cation-cation, cation-anion and anion-anion pairs, respectively, is not restricted by symmetry ($d_{++} = d_{--}$) or additivity ($d_{+-} = (d_{++} + d_{--})/2$) conditions. The system Hamiltonian is:

$$\hat{H} = \sum_i \frac{\mathbf{p}_i^2}{2m_i} + U_N(\{\mathbf{r}_i; i = 1, \dots, N\}) \quad (1)$$

In this equation, $\{\mathbf{p}_i; i = 1, \dots, N\}$ and $\{\mathbf{r}_i; i = 1, \dots, N\}$ represent the momenta and positions, respectively, of the N ions, whose mass is $\{m_i; i = 1, \dots, N\}$ and charge is $\{q_i; i = 1, \dots, N\}$. The potential energy $U(\{\mathbf{r}_i; i = 1, \dots, N\})$ is given by:

$$U_N(\{\mathbf{r}_i; i = 1, \dots, N\}) = \frac{1}{2} \sum_{i \neq j=1}^N v(|\mathbf{r}_i - \mathbf{r}_j|) \quad (2)$$

and:

$$v(|\mathbf{r}_i - \mathbf{r}_j|) = \begin{cases} +\infty & r_{ij} \leq d_{ij} \\ \sum_{i < j}^N \frac{q_i q_j}{\epsilon_0 r_{ij}} & r_{ij} > d_{ij} \end{cases} \quad (3)$$

here $r_{ij} = |\mathbf{r}_j - \mathbf{r}_i|$ is the distance of ions i and j . In what follows, charges are expressed in atomic units, i.e., in units of the (positive) electron charge, while distances will be expressed in units of the cation diameter $d_{++} = 1$. For any extended system, represented by periodically

repeated finite (N ions) samples, overall charge neutrality ($\sum_{i=1}^N q_i = 0$) is strictly required to have a finite electrostatic energy density. For the finite spherical systems that are investigated below, samples may have a non-vanishing net charge $Q = \sum_{i=1}^N q_i$. Again for the sake of simplicity, the simulation procedure is described as it applies to a mono-valent MX salt consisting of cations and anions of the same charge $|q_+| = |q_-| = 1 e$. This restriction is not essential and can be easily removed.

The Hamiltonian in Eqs. 1,-3 is a qualitative but nevertheless relevant model for water solutions of alkali halide salts, and sometimes it has also been used for slightly more complex systems, such as alkaline-earth halide (MX_2) salts¹⁶ in water. To lend some real-life connection to the model, its scaled variables can be transformed to real ones using the following arguments. Based on the evidence from electrochemistry² and also from recent microscopic measurements,¹⁷ cations consists of the bare metal ion accompanied by its hydration shell. The anion, whose hydration shell is far less rigidly bound, consists primarily of the bare halide ion. Because of this assumption, the radius of cations and anions in somewhat asymmetric NaCl or KCl / water solutions is nearly the same, and, following Ref. 11, the common radius is set to $d = 4.25 \text{ \AA}$, which applies to cation-cation, cation-anion and anion-anion pairs. Strictly speaking, this cation-anion symmetry defines the so called *restricted* primitive model, but in the present case, the equality or additivity of the distances of closest approach are only accidental, and no essential change would be required if cations and anions had different diameter, valence (i.e., charge) and relative density. In what follows, all simulations are carried out at $T = 298 \text{ K}$, temperature at which the dimensionless coupling parameter $\beta^* = e^2/(\epsilon_0 d_{++} k_B T)$ is equal to 1.609, which corresponds to low Coulomb coupling. Moreover, the packing fraction $\hat{e} = \frac{\pi \rho}{6} [d_{++}^3 + d_{--}^3]$ of the simulated systems is also low ($5 \cdot 10^{-4} \leq \hat{e} \leq 0.1$), corresponding to relatively dilute electrolyte solution of concentration from 0.01M to 2M. In the expression defining \hat{e} , ρ is the common density of cations and anions. Both conditions of low Coulombic and packing couplings are needed for the application of grand canonical Monte Carlo in the present implementation of the method.

Since water is only implicitly present, the pressure of the particles represents the osmotic pressure only. This might make the samples too compressible to be meaningfully simulated in the NPT ensemble, and the essential inhomogeneity and anisotropy of the interface add to this difficulty. Hence the connection to a precise thermodynamic state is established by using the GCMC formalism, as already done nearly half a century ago for the same model in

Ref. 11. In this scheme, the normal Monte Carlo protocol to update the particles' positions and to sample the phase space of N ions is supplemented by *moves* that attempt to change the number of ions in the system. Normal and grand-canonical moves alternate each other at random, with only the ratio of their relative probability being specified. To keep constant the overall charge in the sample, cations and anions are added or removed in neutral pairs. Since at the simulation conditions the salt molecules are dissociated, the addition of cations and anions occur independently at random positions within the space available to the ions. Also, the cation and anion whose removal is attempted are selected at random among all the ions in the sample. The acceptance probability for addition and removal of ion pairs is easily derived from the analytical expression of the grand canonical partition function for a system at temperature T and chemical potential of the neutral MX molecules $\mu = \mu_+ + \mu_-$. Following again Ref. 11, the addition of a neutral MX salt molecule, increasing by one the number of cations ($N_+ \rightarrow N_+ + 1$) and anions ($N_- \rightarrow N_- + 1$), is accepted with probability:

$$f_{i \rightarrow j} = \frac{1}{(N_+ + 1)(N_- + 1)} \exp[\beta\mu - \beta(U_{N+2} - U_N)] \quad (4)$$

In a related way, removing one MX salt molecule, thus decreasing by one the number of cations ($N_+ \rightarrow N_+ - 1$) and anions ($N_- \rightarrow N_- - 1$), is accepted with probability:

$$f_{i \rightarrow j} = N_+ N_- \exp[-\beta\mu + \beta(U_N - U_{N-2})] \quad (5)$$

As already stated, this approach works satisfactorily only for dilute systems, such as the implicit solvent electrolytes investigated here. This restriction is difficult to remove, but a promising approach to treat concentrated electrolytes such as ionic liquids will be briefly discussed in the last section of this paper.

In the series of simulations described below, the independent thermodynamic variable that uniquely defines the state of the electrolyte solution is the excess chemical potentials in $k_B T$ units $\beta(\mu - \mu_{ideal})$ (here $\beta = 1/k_B T$), which, for a monovalent MX salt, equals $2\langle \ln \gamma_{\pm} \rangle$, where γ_{\pm} is the mean activity coefficient.¹¹ In a preliminary stage of the computation, this quantity has been determined by GCMC as a function of the molarity M of the electrolyte solution, then used in the following stages to fix the thermodynamic state of the bulk system in equilibrium with the inhomogeneous electrode / electrolyte sample.

The second crucial element in the model electrochemical cell is the metal electrode, able to transfer electrons between the two sides of the interface. The simplest extension of the primitive

electrolyte model to investigate the electrified interface consists of a system in which the charged hard sphere ions are confined between two structureless planar parallel surfaces impenetrable by the ions, and carrying a surface charge density σ in $[e/d_{++}^2]$ units. This paradigmatic model has been simulated several times in the past (see, for instance, Ref. 14,18,19), providing a wealth of information on simple electrified interfaces as a function of electrolyte concentration and surface charge density, including the electrostatic potential drop across the interface, the differential capacitance, the density profile of the electrolyte ions along the direction perpendicular to the planar surface, the specific adsorption of ions on the metal electrodes. The scheme, however, has one drawback, since necessarily it introduces two electrodes and two interfaces, which, away from the PZC, may become inequivalent, unless the electrodes and ions are both symmetric. Given the (still) microscopic sizes of the simulated samples, disentangling the properties of the two electrified interfaces might become uncertain. In real-life, macroscopic systems, both interfaces are in equilibrium with a common bulk, and, although related, do not interact directly with each other. Ideally, it would be advantageous to deal with half of the electrochemical cell at a time, which is in fact a conceptual idealisation widely used in electrochemistry. For this reason, we resort to a variant of the basic model in which the electrolyte is enclosed into a spherical surface of radius R_e which plays the role of the unique electrode in the half cell. Then, the state of the electrolyte is identified and kept stationary in time by the GCMC approach, offsetting the effect of the finite sample size, and also of the electrostatic bias and electric current flowing through the electrode. Needless to say, the disadvantage is that the single-electrode model introduces a curvature dependence of the results, which however, can be estimated and compensated. This aspect will be discussed in the following sections and in the Supplementary Information (SI) document.

The finite and inhomogeneous samples under investigation will be simulated under charge control, as opposed to other methods that describe systems under electrostatic potential control,^{20,21} whose comparison with experiments might be more direct. However, the electrostatic properties of the curved interfaces simulated in the present study, such as the surface charge, the electrostatic potential drop across the interface, the screening length and the interfacial capacitance, have been quantitatively determined, in such a way that the results obtained under charge-control conditions can be translated into the potential-control picture.

To mimic real systems, the surface charge density on the spherical electrode would exactly

balance the overall charge of the electrolyte inside the spherical cavity:

$$\sigma = \frac{-\left(\sum_{i=1}^N q_i\right)}{4\pi R_e^2} \quad (6)$$

In the single electrode model, the non-vanishing σ does not play an explicit role, but it is implicitly accounted for by introducing a charge imbalance on the electrolyte side of the interface. This initial charge is left unchanged by the GCMC that adds or removed neutral pairs of ions. Because of Gauss's theorem, the correct electric field condition $E_r = 4\pi\sigma$ at the interface is automatically satisfied, provided the charge density distribution is, on average, spherically symmetric both on the metal and the electrolyte sides of the interface. This observation reflects the fact that the electric field due to a homogeneously charged spherical surface identically vanishes on its inside.

It is important to remark that the electrostatic field conditions at the interface are not rigorously treated, even at the simplest (perfect conductor) level of image charge. However, image charges can easily be computed for spherical conducting interfaces²² and their effect can be accounted for by a slight extension of the model.

The novel aspect of the present model consists of a new type of move that introduces the electron transfer across the metal / electrolyte interface, as well as a protocol intended to match this process with the underlying diffusion of the ions that keeps the system in a stationary state, despite the change of ions' concentration in the immediate vicinity of the electrode driven by the electron transfer itself.

As stated in the introduction, we will be looking at cations which may closely approach the cathode, picking up an electron thus reducing their positive charge by one unit. The simplest model for the electronic part of the process, in which electrons move from the metal valence band to ionic/atomic states, corresponds to a stochastic surface hopping picture.^{23,24} This assumes that the quantum mechanical electron jump takes place instantaneously, after a latency representing the time needed to overcome the free energy barrier between the initial and final state (see below), and accounting also for the probabilistic nature of quantum transitions. The kinetics of the process corresponds to that of first order chemical reaction,³ whose rate is proportional to the abundance of ions of the reactive species (cations, in this case) located within a distance δR from the metal surface such that the transition probability is not vanishingly small.

The present model characterises the inherent kinetics of the electron transport through the

interface by the parameter k_e , expressing the rate of the electron transfer from the cathode to a single active cation. The aim of the model is to determine how this basic rate combines with all the other many-ion effects to produce the flow of charge through the system. This output quantity, which, in the following, will also be referred to as the *overall electron transfer rate*, has the dimension of a current density, being expressed as charge transferred per unit area and unit time.

The k_e parameter can be computed by quantum perturbation theory,⁷ provided the coupling of the two sides is weak, or by many-body methods based, for instance, on the Anderson-Newns Hamiltonian.^{25,26} For the sake of simplicity, in what follows, it is assumed that the top of the electrode valence band has *sp* character, hence the corresponding valence density of states is broad (*wide band assumption*) and below the Fermi level it changes slowly with energy. Then, despite the fact the cation has an energy spectrum of sharp levels, the rate will depend weakly on the bias, and will not display the resonance spikes expected for electrodes made of transition metals. Instead, the dependence of the transfer rate from the metal-ion separation, which could also be computed by the same electronic structure methods, is strong, as suggested from the fact that, according to perturbation theory, k_e depends on the superposition of the electronic wave functions centred on the metal and on the ions, which decays exponentially with increasing their mutual distance. Hence, the model will only include the charge transfer for the ions whose radial distance δR from the electrode is of the order of the Å. In principle, k_e accounts for electronic effects only, resulting from the activation (free) energy ΔG of electronic origin, that characterises the kinetics of the reaction between the metal and the bare cation, which might be seen as a tunneling process. However, in schematic models like the present one, other effects might be folded into the definition of k_e . For instance, the electron transfer often involves a positive *reorganisation energy* λ , which is the free energy barrier associated with the loss (or, at least, drastic reorganisation) of the tightly bound hydration shell of the cation being neutralised. Hence, the total activation energy E_{act} that is responsible for the k_e determination is:⁴⁻⁶

$$E_{act} = \frac{(\lambda + \Delta G)^2}{\lambda} \quad (7)$$

which may easily reach and surpass the eV energy scale. Hence, in most cases the electron transfer is a relatively slow process, whose rate per ion typically will be below the inverse nanosecond. The time step of atomistic molecular dynamics simulations is of the order of the femtosecond, implying that more than 10^6 MD updates of forces, velocities and positions are

needed per every event (on average) on each particle within the jump distance. Of course, a large interface will involve many active particles, whose number grows like the interfacial area, increasing the rate of statistics accumulation. Since, however, the computational cost per step grows approximatively like the square of the number of particle, increasing the sample size does not provide a scaling advantage.

To account for all these aspects in the simplest possible way, the k_e in the present study is a free parameter to be varied in order to investigate the model properties. Moreover, in the present model, the same rate constant k_e is attributed to all cations located within a distance $\delta R = d_{++}/2$ from the metal surface. Each cation satisfying this distance condition has the following probability to be still unreacted at time t :

$$p_{survival}(t) = \exp[-k_e t] \quad (8)$$

For any given cation residing in the active region, the time to (first) neutralisation is a random variable Δt whose distribution $p(\Delta t)$ is:

$$p(\Delta t) = k_e \exp[-k_e t] \quad (9)$$

In this way, the lifetime of a cation adsorbed on the electrode within the distance δR turns out to be $\tau = k_e^{-1}$. Simulating this process is the same as simulating the radioactive decay of an assembly of metastable nuclei, or the de-excitation of metastable electronic excited states. In these analogous cases, the probability distribution in Eq. 9 is interpreted as describing the first escape time out of a metastable minimum. This same decay/relaxation picture is reminiscent of the way kinetic Monte Carlo simulates the system escape from any given free energy basin of the system under consideration.¹³ In a broader context, the kinetic approach to describe all these processes are based on the theory of the master equation.²⁷ A variety of algorithms²⁸ and also computer codes are available for this type of simulations.

The crucial aspect of the method that is proposed below is the matching of the stochastic charge transfer process with the second dynamical process, i.e., the self-diffusion of the electrolyte ions, that is needed to keep the system in a stationary state. The problem addressed by the discussion that follows is how to join these two components of the dynamics, mixing them in the right proportion that reproduces the mutual effects they have on each other. The electron transfer itself already has its own real time clock, whose beat is given by k_e^{-1} . Then, the idea is to use the ions' diffusion coefficient computed or measured in real time to set up a

time scale for the response of the electrolyte density distribution to the disturbance due to the flow of charge through the system.

Then, the synchronisation of the stochastic transfer of electrons at the interface with the Brownian dynamics of ions in the electrolyte solution is achieved through the following steps. First, the mean square displacement per ion $\langle |\mathbf{r}_i(\tau + \tau_0) - \mathbf{r}_i(\tau_0)|^2 \rangle_{MC}$ as a function of the time interval τ is evaluated for all the samples of interest. Here τ is the MC time, measured in MC steps, and *sweep* consists of a complete sweep of attempted MC moves over all ions. To be precise, following standard practice and for the reasons discussed below, the ions whose displacement is attempted are selected at random. Therefore, the *sweep* term will only be used as a concise way to denote a number of attempted moves equal to the number of particles. It will not imply, in particular, that during a sweep each ions will be tested for displacement, or, much less, that each atom is displaced only once or event at all during a sweep. In the definition of the average displacement, the $\langle \dots \rangle_{MC}$ notation indicates averaging over the initial time τ_0 and also over all ions of the sample.

In a fluid system, the Metropolis Monte Carlo dynamics results in a diffusive regime in which the mean square displacement of particles asymptotically grows linearly with MC time τ . Then, the self-diffusion coefficient D_{MC} of ions in MC time is defined through the same Einstein's relation that defines the real time diffusion D :

$$D_{MC} = \frac{1}{6} \lim_{\tau \rightarrow \infty} \frac{\langle |\mathbf{r}_i(\tau + \tau_0) - \mathbf{r}_i(\tau_0)|^2 \rangle_{MC}}{\tau} \quad (10)$$

Needless to say, D_{MC} depends on the electrolyte concentration in solution, and on the step Λ of the attempted MC single-ion moves along each Cartesian direction, in analogy with the real-time diffusion coefficient D which depends on the electrolyte concentration and on the mass of the diffusing particles. Notice that for the symmetric electrolyte model, only one diffusion coefficient is needed. The discussion and ensuing simulation protocol could easily be extended to cover the more realistic case of an asymmetric electrolyte, which will require two different steps for cations and anions to reproduce their two distinct diffusion constants.

The correspondence between real (δt) and MC ($\delta \tau$) time is established by stating that the δt and $\delta \tau$ intervals are equivalent if the increase of the mean square displacement per ion is the same in the two cases. Starting from the Einstein's relation, it is easy to verify that this condition is equivalent to impose that:

$$\delta t = \delta \tau \frac{D_{MC}}{D} \quad (11)$$

where δt , $\delta\tau$, D , and D_{MC} are expressed in their own units, for instance, nanoseconds, MC steps, $\text{\AA}^2/\text{ns}$ and $\text{\AA}^2/\text{MC step}$, respectively.

Then, the knowledge of the real time diffusion coefficient for the same system that is being investigated by MC is required to define the correspondence between the MC time and real time. Ideally, one would use the real-time diffusion coefficient computed by molecular dynamics for the same model investigated by MC. Since, in the present case, the implicit-solvent, hard sphere model is not likely to have a real-time diffusion constant comparable to those of alkali halide solutions, we use, or, better, approach the experimental self-diffusion constants of Na^+ and Cl^- reported in the literature as a function of temperature and electrolyte concentration. The diffusion properties of Na^+ and Cl^- will be symmetrised by introducing the average diffusion coefficient $D = \sqrt{D_+ D_-}$. Starting from these considerations, the protocol used to relate the real and MC time is fully defined in the Results sections, where diffusion coefficients and computational parameters are listed and discussed.

In what follows, $\delta\tau$ will represent the unit MC time (i.e., one MC step), while δt will represent the corresponding real time interval, expressed, in the present case, in ns. In other terms, δt is the real time covered by a set of N attempted MC moves, where, as before, N is the number of ions. As already stated, for any given electrolyte concentration, the diffusion coefficient in MC time depends on the amplitude Λ used, along each Cartesian coordinate, for the MC attempted single ion displacement. In dilute systems, whose dynamics is virtually Brownian, D_{MC} will scale nearly quadratically with this step amplitude. Slight deviations from this simple law are due to the dependence of the MC acceptance / rejection probability on Λ (see Sec. S1 in SI). The overall near quadratic dependence gives a suitable handle to tune δt : increasing Λ increases D_{MC} , and thus increases δt by the same nearly quadratic ratio. If δt is too short, the advantage of the MC dynamics with respect to molecular dynamics is reduced. If δt is too long, the time resolution of the method is low, and might introduce artifacts in the combined electron transfer versus ionic diffusion dynamics.

It might be worth emphasizing that the full sweep of N attempted single-particle MC moves has been introduced as a unique and indivisible unit of time. The reason of this choice is that in this way $\delta\tau$ is certainly long enough to allow the system to lose memory of its previous state at each step, fulfilling all requests of Markovian evolution and purely diffusive behaviour. However, as already said, particles are not moved in a regular order, but each attempted move is applied to an ion chosen at random. Hence, during one $\delta\tau$ (i.e., what we called a *sweep*), it

might happen that a given ion is moved more than once, and certainly many ions do not move even once. The random choice of the ion makes the flow of time more uniform, and allows to split the unit of time $\delta\tau$ in sub-units, corresponding to a fraction n of the N attempted moves. This might be needed to increase the time resolution at low ion density, when diffusion is so fast to correspond to long δt values. This choice, which is less rigorous than the previous one since it does not fully guarantee the loss of memory from one step to the next, is nevertheless exploited in the computations presented in Sec. III.

Taking into account all these aspects, the MC simulation will proceed according to the following block diagram:

1. Electron transfer simulations are started from one configuration selected at random from the GCMC simulation of the sample, and the system time t_s is initialised to zero. All cations in contact with the electrode (say, within a skin distance δR) are initialised with a label (i.e., a binary state variable) which says that they are *active*, i.e., in the process of negotiating the charge transfer, whose rate, per cation, is k_e . Also, a random variable t_e is associated to each of these active ions, drawn from the exponential distribution $p(t) = k_e \exp[-k_e t]$. The t_e variable, different for each cation, gives the first passage time for their change of oxidation state, which, in what follows, will also be indicated as the ion *expiration* time. In other terms, this random variable tells when each ion will change state, provided it remains active in the meantime. This expiration time is not initialised for inactive particles.
2. The simulation is carried out by performing a MC step consisting of N attempted displacements (or over a subset of n attempted displacements) of ions chosen at random. At the end, the system time is advanced by the corresponding real time δt (or $n\delta t/N$).
3. The expiration time of each *active* ion is compared with the new time. If the accumulated system time is longer than the expiration time, the ion undergoes the charge transfer, carried out as detailed below. If the accumulated time is shorter than the expiration time of the given ion, this one will continue accumulating time as an active ion.
4. New ions might have entered the active range during the diffusion stage. Their binary state variable is turned to *active*. For each of them, a random variable t_r is drawn from the exponential probability distribution, and their expiration time is set to $t_s + t_r$.

5. Steps 2, 3 and 4 are repeated until the accumulated system time exceeds the preset value.

In applying this algorithm, the following simplifying assumptions are made about the system and the electron transfer process. Since the electrode/electrolyte model is very idealised, and does not target any specific system, both the electron transfer rate and its distance dependence will be decided a priori, without resorting to an electronic structure computation. In particular, the rate will be the same for all ions of the reactive type (cations, in the present case) located within one ionic radius ($\delta R = d_{++}/2$) from the metal electrode surface. The value of the rate per active ion will be used as a parameter to simulate low-flow (0.01 ns^{-1}) / high-flow (0.1 ns^{-1}) conditions. The attempted electron transfer is accepted a priori, without any acceptance/rejection stage, based, for instance, on the energy change. This is because the scale of the electron energy change is supposed to be much higher than thermal energy, hence the process is driven by the electro-motive force exerted on the half cell by the external circuit.

In the present model, no detailed chemical reaction is specified for all the ions during the flow of current through the half cell. This aspect might be added at a later time to extend the scope of the model and to apply it to a specific problem. Right now, the change that the active ions undergo upon changing their oxidation state is used to model some additional condition on the system evolution. In the present study, the electron transfer mechanism has been tuned in order to drive a current density $\mathbf{j}(\mathbf{r})$ through the systems whose radial component $j_r(\mathbf{r})$ is, on average, uniform over the electrode cavity. Of course, *radial* refers to the spherical polar coordinate system concentric with the spherical electrode. This request has been made to mimic the homogeneous distribution of current density at planar interfaces, and has been fulfilled in the following way. First, the cation which is undergoing neutralisation is removed, i.e., turned into a neutral particle which is only implicitly represented by the model (like the solvent molecules). Instead, a cation is randomly inserted at a new random position \mathbf{r}_n within the volume enclosed by the spherical electrode. The new position \mathbf{r}_n is selected with probability $p_r(r_n)$ which is not uniform, but, ideally, depends on $r_n = |\mathbf{r}_n|$ as $1/r_n$. In this way the radial current density is predicted to be the same through all spherical surfaces concentric with the electrode. However, the probability $p_r(r_n)$ is singular and non-integrable at the origin. To avoid this problem, the (unnormalised) probability distribution p_r is slightly modified into:

$$p_r(r) = \frac{1}{1+r} \quad (12)$$

and it has been verified that in this way the radial component of $\mathbf{j}(\mathbf{r})$ is virtually uniform

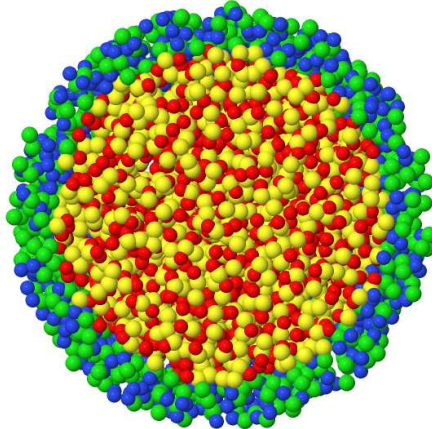


FIG. 2: Snapshot of the smallest ($N = 4000$) and most concentrated ($2M$) sample. Red and yellow dots represent cations and anions, respectively, in the inner sphere, accounting for 51.2 % of the volume; blue and green dots represent cations and anions, respectively, in the outer sphere, accounting for the remaining 48.8 % of the volume. The radii of the ions are not on scale with the radius R_e of the spherical electrode. The target molarity is tuned on the inner sphere only, but the GCMC addition and removal of ion pairs is carried out over the entire volume (see Sec. II.

over the whole sample (See the Results section). If, in the new location, the inserted cation is superimposed to any other ion, a new random position is selected, until the move is successful. In this sense, as we already wrote, the move occurs a priori.

In a different scenario, a fraction $0 \leq \nu \leq 1$ of the neutralising ions is exchanged with an anion chosen at random from the entire anion population. The remaining $(1 - \nu)$ fraction of neutralising ions will undergo the same relocation process describe before. Both processes are weighted with the probability p_r defined in the previous sentence, applied to the new position of the interchanged/relocated cation, or to the old position of the interchanged anion. This combination of simple relocation and cation/anion exchange will result in the simultaneous presence of a cathodic and anodic current through the system, whose relative strength depends on ν . Both currents turn out to be homogeneous across all spherical surfaces concentric with

the electrode, as homogeneous is the net current in systems delimited by planar interfaces.

Two remarks are in order. First, the condition of (nearly) uniform radial current density $j(\mathbf{r})$ over the whole sample implies a violation of the continuity equation, whose origin and impact are discussed in the Results section. Second, the transformation of the neutralising cation into a neutral particle only implicitly represented in the model is somewhat artificial. This choice has been made in the present study for the sake of simplicity only. In further developments of the method, the transforming ions could contribute to the growth of the electrode through an electro-deposition process, or could take part in some more complex electrochemical reaction, opening the way to simulating Galvanic or fuel cells. The further redox reactions required to model these systems and phenomena could be treated in analogy with the electron transfer at the electrode/electrolyte interface.

III. RESULTS

A. Sample preparation and characterisation of the electrode/electrolyte interface

At first, neutral samples have been prepared to represent spherical electrode / electrolyte solution interfaces whose fluid side is in equilibrium with electrolyte solutions of concentration (molarity) $M=0.01; 0.1; 0.5; 1; \text{ and } 2$. To assess size (and therefore curvature) effects, each concentration has been simulated at three sizes, corresponding to $N/2 = 2000, 4000 \text{ and } 8000$ neutral ion pairs, with N being the number of ions in the sample. To be precise, these round N values are the *nominal* numbers of ions in the sample, meaning that the sample volume contains precisely those numbers of ions at the target molar concentrations. However, the actual average number might differ slightly because of fluctuations due to the grand-canonical MC method and because of the perturbation represented by the fluid/solid interface, that is measured by the adsorption coefficients Γ_+, Γ_- for cations and anions, respectively (see Tab. I). All simulations have been carried out at $T = 298 \text{ K}$, with water being represented by a (relative) dielectric constant $\epsilon_0 = 78.5$.

The sample preparation consisted of the following steps. Since the molarity (M) times the Avogadro number \mathcal{N}_A gives directly the number density of molecules per liter of solution, the volume V of each spherical sample is set to:

$$V = \left(\frac{N}{2}\right) \frac{1}{M\mathcal{N}_A} \quad (13)$$

TABLE I: Geometric, thermodynamic, structural and electrostatic properties of the neutral simulated systems. M: molarity concentration of the electrolyte in the water solution in equilibrium with the spherical interface; N: *nominal* number of ions, see Sect. III A; R_e : radius of the spherical interface; $2\langle \ln \gamma_{\pm} \rangle = \beta(\mu - \mu_{ideal})$: excess chemical potential of an ion pair. γ_{\pm} is the mean ionic activity; $\Gamma_+ = \Gamma_-$: adsorption coefficient of cation and anions expressed in number of ions per unit area (d_{++}^2), which are equal in the case of neutral electrode ($\sigma = 0$); $\rho_+(R_e) = \rho_-(R_e)$: ionic number density at contact with the electrode, expressed in number of ions per unit volume (d_{++}^3). The determination of these quantities from the raw simulation data is detailed in Sec. S2 of SI.

M	λ_{DH}/d_{++}	N	R_e/d_{++}	$2\langle \ln \gamma_{\pm} \rangle$	$\Gamma_+ = \Gamma_-$	$\rho_+(R_e) = \rho_-(R_e)$
2	1.043	4000	17.28	0.522 ± 0.003	$(5.8 \pm 0.4) 10^{-3}$	0.1247 ± 0.0004
		8000	21.78	0.524 ± 0.003	$(5.8 \pm 0.4) 10^{-3}$	0.1262 ± 0.0004
		16000	27.44	0.524 ± 0.003	$(6.3 \pm 0.4) 10^{-3}$	0.1249 ± 0.0007
1	1.475	4000	21.78	-0.252 ± 0.003	$(1.1 \pm 0.2) 10^{-3}$	0.0509 ± 0.0002
		8000	27.44	-0.258 ± 0.003	$(0.88 \pm 0.2) 10^{-3}$	0.0507 ± 0.0003
		16000	34.57	-0.258 ± 0.004	$(0.78 \pm 0.2) 10^{-3}$	0.0510 ± 0.0003
0.5	2.086	4000	27.44	-0.492 ± 0.004	$-(3.5 \pm 1) 10^{-4}$	$0.02298 \pm 5 10^{-5}$
		8000	34.57	-0.496 ± 0.004	$-(4.2 \pm 1) 10^{-4}$	$0.02288 \pm 5 10^{-5}$
		16000	43.55	-0.490 ± 0.004	$-(4.4 \pm 1) 10^{-4}$	$0.02293 \pm 8 10^{-5}$
0.1	4.665	4000	46.92	-0.440 ± 0.004	$-(2.6 \pm 0.3) 10^{-4}$	$4.332 10^{-3} \pm 2 10^{-5}$
		8000	59.11	-0.446 ± 0.004	$-(2.5 \pm 0.2) 10^{-4}$	$4.312 10^{-3} \pm 5 10^{-5}$
		16000	74.47	-0.447 ± 0.004	$-(2.8 \pm 0.3) 10^{-4}$	$4.376 10^{-3} \pm 2 10^{-5}$
0.01	14.75	4000	101.08	-0.1958 ± 0.001	$-(2.8 \pm 0.2) 10^{-5}$	$4.451 10^{-4} \pm 2 10^{-6}$
		8000	127.35	-0.1970 ± 0.001	$-(3.1 \pm 0.2) 10^{-5}$	$4.486 10^{-4} \pm 3 10^{-6}$
		16000	160.45	-0.1945 ± 0.001	$-(3.0 \pm 0.2) 10^{-5}$	$4.501 10^{-4} \pm 1 10^{-6}$

with the result being expressed in litres.

Each sample is progressively filled by grand canonical MC (see Sec. II), using the excess chemical potential as the independent variable that controls the average density, and thus the

thermodynamic state of the sample. To be precise, the target density is imposed not on the total volume, but only on the central portion corresponding to 51.2 % of the volume (up to 80% of the radius), since the density of the external portion, accounting for the remaining 48.8 % of the volume, might be slightly affected by the specific adsorption of ions at the electrode surface. This subdivision of the volume and of the particles it contains is illustrated in Fig. 2.

The primary thermodynamic quantity determined in these computations has been the mean ionic activity coefficient γ_{\pm} , whose logarithm is related to the excess chemical potential of the two ion species according to the equation:

$$2\langle \ln \gamma_{\pm} \rangle = \beta(\mu - \mu_{ideal}) \quad (14)$$

where $\mu \equiv \nu_+ \mu_+ + \nu_- \mu_-$, with ν_+ , ν_- giving the stoichiometry of the $M_{\nu_+} X_{\nu_-}$ electrolyte compound. As already stated, in the present case, $\nu_+ = \nu_- = 1$. The results of this sample preparation stage are summarised in Tab. I.

The main result coming from the data reported in Tab. I is that $2\langle \ln \gamma_{\pm} \rangle$ shows, as expected, a marked dependence on the electrolyte concentration, but a low dependence on sample size. This observation suggests that the protocol described above defines a unique bulk electrolyte solution in equilibrium with the interfaces of different curvature. Remarkably, the results agree to within the error bar with the results of Ref. 11 despite the large difference of sample size and length of the GCMC simulations, that reflects the vast improvement of computational equipment of the last 40 years. All these observations somewhat justify the usage of the spherical electrodes, and downplay the effect of curvature on the results.

Then, simulations have been extended to charged samples, starting from the neutral ones, and changing a priori the $+/-$ charge of the ions until reaching the target charge imbalance, at the same time tuning the overall chemical potential to conserve the $2\langle \ln \gamma_{\pm} \rangle$ value of the sample. The slight tuning is needed because, at equal volume, neutral and charged samples contain somewhat different numbers of particles, hence the ideal contribution to the overall chemical potential (entering the GCMC acceptance probability) is slightly different. After this short calibration, the grand canonical part of the simulation proceeds as before with the attempted addition and removal of neutral ion pairs that maintain the total charge of the sample. The results of these preliminary GCMC simulations for neutral and charged samples have been analysed to collect data on the structural and thermodynamic properties of the interface, and also on the dependence of these properties on the surface curvature and surface charge density σ .

TABLE II: Properties of the electrostatic double layer as a function of electrolyte concentration, surface charge and size of the sample. Slight variations in the surface charge for sample of different size are due to the fact that the charge is quantised in units of e .

M	R_e/d_{++}	R_e [Å]	σd_{++}^2	$\Delta\varphi = \beta e \langle \varphi(R_e) - \varphi(0) \rangle$
2	17.28	73.44	-0.05328	-0.2905 \pm 0.01
	21.78	92.55	-0.05336	-0.3005 \pm 0.002
	27.44	116.61	-0.05328	-0.2636 \pm 0.005
2	17.28	73.44	-0.10655	-0.6516 \pm 0.003
	21.78	92.55	-0.10673	-0.5999 \pm 0.002
	27.44	116.61	-0.10656	-0.5767 \pm 0.006
0.1	46.92	199.39	-0.07205	-0.3527 \pm 0.004
	59.11	252.22	-0.07243	-0.3582 \pm 0.001
	74.47	316.52	-0.07231	-0.3446 \pm 0.006
0.1	46.92	199.39	-0.01441	-0.6870 \pm 0.004
	59.11	252.22	-0.01448	-0.6885 \pm 0.001
	74.47	316.52	-0.01446	-0.6865 \pm 0.006
0.01	101.08	429.58	-0.00312	-0.2428 \pm 0.001
	127.35	541.24	-0.00312	-0.2548 \pm 0.001
	160.45	681.91	-0.00312	-0.2366 \pm 0.005
0.01	101.08	429.58	-0.00312	-0.5210 \pm 0.001
	127.35	541.24	-0.00312	-0.4994 \pm 0.002
	160.45	681.91	-0.00312	-0.4951 \pm 0.004

Here we only summarise the features that are relevant for the conductivity simulations. Further results, such as the electrostatic screening length and interfacial capacitance, are collected and briefly discussed in Sec. S3 of the SI document.

For what concerns the electron transfer process and the ensuing electrical conductivity through the system, the major structural information from the preliminary simulation stage is given by the number and charge density profiles of the ions close to the metal surface, since

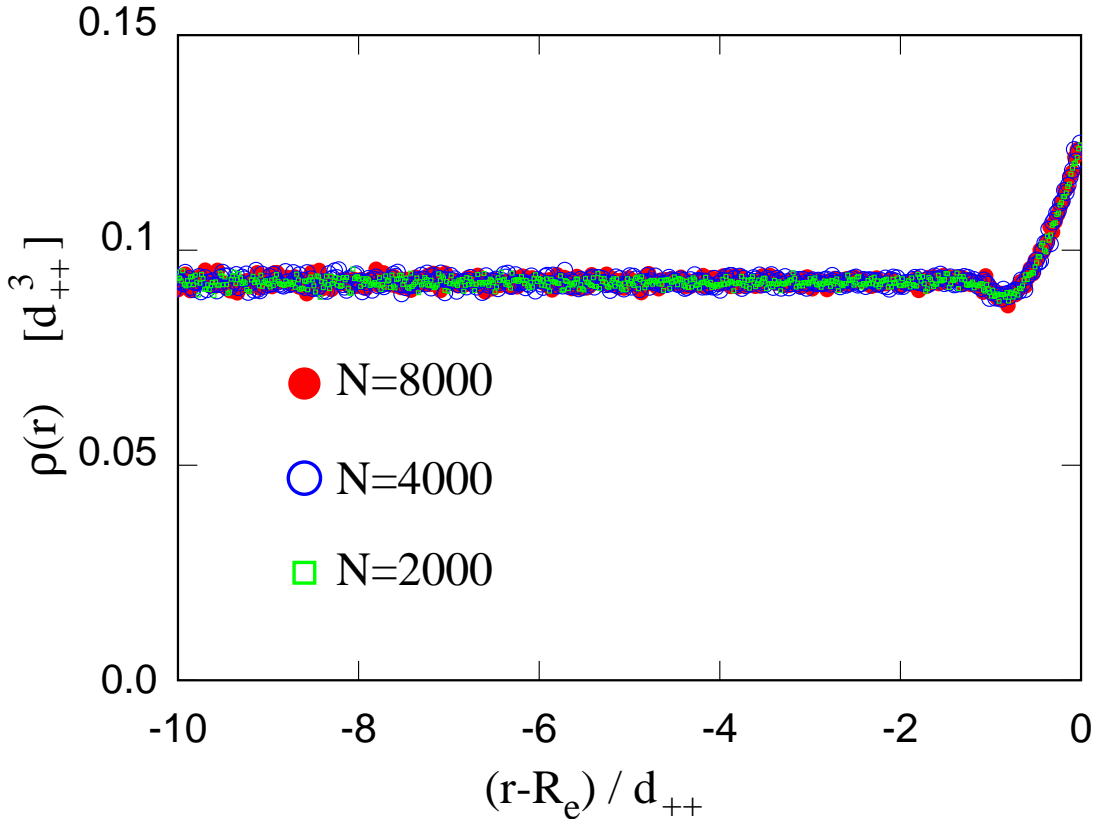


FIG. 3: Size dependence of the density profile for the neutral systems ($\sigma = 0$) at 2M concentration.

these determine the number of active ions and thus the observed rate of electron transfer. First, it has been verified that, over the range of sizes covered by the present study, the density profiles are nearly independent from the curvature of the metal electrode (See Fig. 3).

Then, the dependence of the ionic density profiles on the surface charge density σ , has been analysed, focusing the attention on their properties in the immediate vicinity of the electrode. As already repeatedly stated, the overall state of the system is fixed by imposing the $2\langle \ln \gamma_{\pm} \rangle$ value of the whole spherical sample. Then, charged and neutral samples belong to the same thermodynamic state if they are in equilibrium with the same (neutral) bulk, identified by the value of $\beta(\mu - \mu_{ideal}) = 2\langle \ln \gamma_{\pm} \rangle$. It turns out that, if this condition is satisfied, the molarity

TABLE III: Inverse differential capacitance C_D^{-1} (in d_{++} units) as a function of system size and electrolyte concentration. C_D^{-1} is computed by differentiating a linear interpolation of the data for $\langle\varphi(R_e) - \varphi(0)\rangle$ as a function of σ using the data in Tab. II.

N	2M	1M	0.5M	0.1M	0.01M
4000	5.72	10.76	18.96	47.67	167.23
8000	5.62	11.84	18.68	47.54	160.02
16000	5.41	11.43	18.24	47.47	158.92

of the inner sphere (as before, the central 51.2% of the spherical volume) is the same to within the error bar, confirming that the perturbation due to the surface charge is quickly screened by the redistribution of the ionic density profiles. Simulations have been limited to a rather narrow range of surface charge densities ($|\sigma| d_{++}^2 \leq 0.2$), which are the most relevant in electrochemical devices. The results are reported in Tab. II and Fig. 4, and discussed in more detail again in Sec. S3 of the SI document.

At a planar interface, the contact density depends on the surface charge according to the exact relation²⁹ expressing mechanical equilibrium normal to the interface:

$$k_B T \sum_{\alpha} \rho_{\alpha}(R_e) = P + \frac{2\pi\sigma^2}{\epsilon_0} \quad (15)$$

where P is the pressure of the bulk solution in equilibrium with the interface, $\alpha = +, -$ labels the two ion species, and σ is the surface charge. The last term, in particular, can be identified as the pressure of the electric field at the interface as given by the Poynting vector.³⁰ Hence, for a neutral interface, the value of the electrolyte density (translated in kinetic pressure units) at contact tends to the bulk osmotic pressure, apart, possibly, from a correction due to the surface curvature. The value of this contact density, always for neutral interfaces, is listed in Tab. I. While we did not try to analytically derive the curvature dependence of the contact density, it has been verified that this dependence cannot be detected in the simulation results of Tab. I, despite long runs and small statistical error bars. Moreover, the simulation results for neutral interfaces show that the contact between the electrode and the electrolyte turns from weakly non-wetting to wetting with increasing molarity M (See Sec. 4 of SI), reflecting the change of the excess pressure (i.e., the deviation from the ideal gas value $k_B T \rho$) from negative to positive.

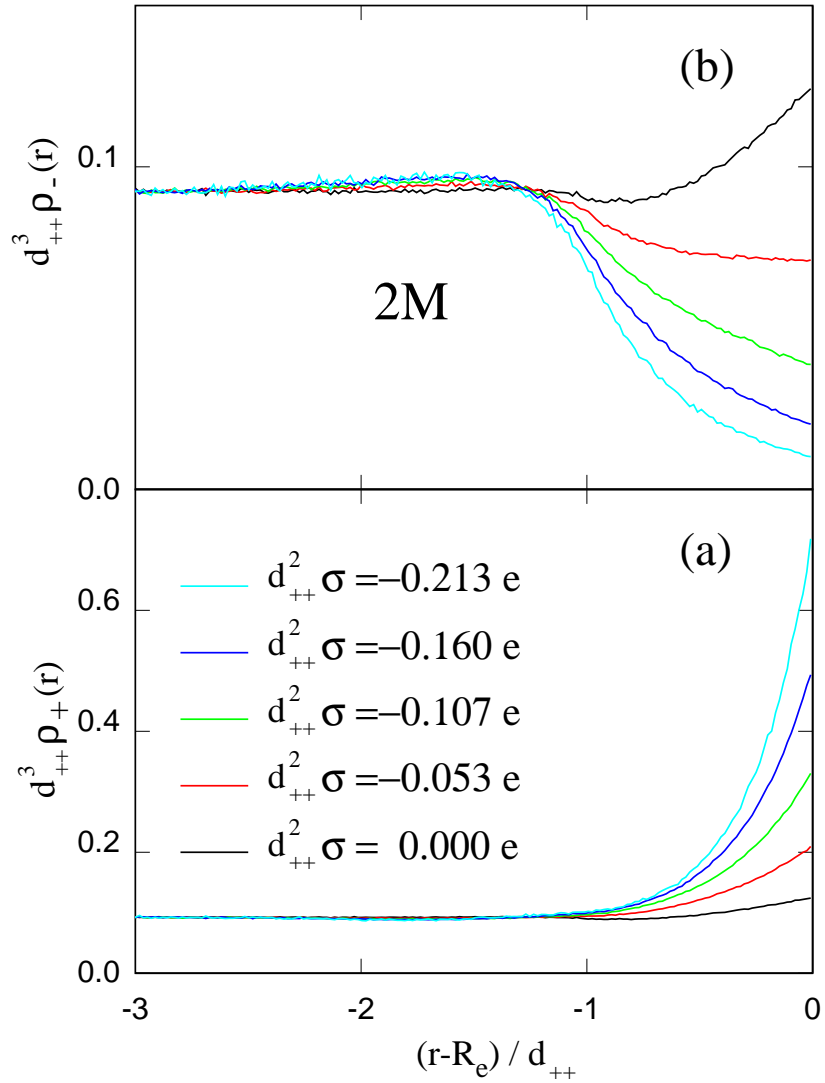


FIG. 4: Dependence of: (a) cation and (b) anion density profile as a function of the surface charge density σ . Notice the change of scale between panel (a) and (b). Electrolyte concentration of the equilibrium bulk phase: 2M.

Needless to say, this model results might not hold for real systems, since it refers to the osmotic pressure only, and disregards the essential role of water in electrolyte solutions.

Of particular interest for the conductivity simulation is the dependence of the contact density on the surface charge. According to Eq. 15, the sum of cation and anion densities at contact

grows quadratically with the surface charge. The simulation data for the charged interfaces satisfy this relation to within the error bar (See Fig.S6 in Sec. 4 of SI). The same data also show that, as soon as $|\sigma|$ is not very low ($|\sigma| \geq 0.1$), only the majority species contributes significantly to the contact density. In the case of the simulated samples, the ions participating in the redox activity are the cations, whose contact density as a function of σ displays a marked asymmetry with respect to the $\sigma = 0$ state, which, by definition corresponds to the potential of zero charge. The $\rho_+(R_e)$ dependence on σ , in particular, will be nearly quadratic when $\sigma \ll 0$, while it will decrease only slowly with σ increasing above zero. This behaviour will be verified and further discussed in the following subsection.

A second quantity that might greatly affect the electron transfer process at the interface is the electrostatic potential drop across the interfacial double layer, which, assuming that the charge distribution is (on average) spherically symmetric, is given by:

$$\langle \varphi(R_e) - \varphi(0) \rangle = \frac{Q}{R_e} - 4\pi \int_0^{R_e} r \rho_Q(r) dr \quad (16)$$

where R_e is the radius of the spherical cavity enclosing the electrolyte solution. Collecting statistics for $\rho_Q(r)$ on a grid gives a practical way to compute $\langle \varphi(R_e) - \varphi(0) \rangle$ by a simple 1D integration, which, however, is necessarily affected by the error of discretising $\rho_Q(r)$ on a grid. An approach which does not suffer from this limitation is easily obtained. Since:

$$\rho_Q(r) = \langle \hat{\rho}_Q(\mathbf{r}) \rangle = \left\langle \sum_{i=1}^N q_i \delta(|\mathbf{r}_i| - r) \right\rangle \quad (17)$$

one has:

$$\varphi(R_e) - \varphi(0) = \frac{Q}{R_e} - \left\langle \sum_{i=1}^N \frac{q_i}{r_i} \right\rangle \quad (18)$$

upon interchanging the integration and the averaging operations.

Therefore, the electrostatic potential drop can be computed by averaging on the fly $\sum_{i=1}^N \frac{q_i}{r_i}$, where r_i is the radial component of the position vector in a spherical coordinates systems whose origin is the centre of the spherical cavity. The $\sum_i q_i/r_i$ estimator has the obvious problem that it is bound neither from below nor from above, since ions can approach the origin without limitations. Hence, the variance might be very large, although the probability of very high or very low contributions to the estimator is vanishingly small, being weighted by the $r^2 dr$ volume element. A variety of other estimators for the same quantity could be tried, but we did not pursue this electrostatic investigation any further at this stage.

TABLE IV: Conversion table of MC time (τ , MC steps) into real time (δt , ns). Λ is the amplitude of the MC step along each Cartesian coordinate. The error bars on computed properties such as the acceptance ratio $\langle \xi \rangle$ of MC steps and the diffusion coefficient in MC time are listed explicitly. The error bar on the derived quantity $\delta t/\delta \tau$ is indicated implicitly by the number of digits in the quoted result. The conversion from scaled units to real units is carried out by assuming $d_{++} = 4.25 \text{ \AA}$, and a constant real time diffusion coefficient D of $1 \cdot 10^{-5} \text{ cm}^2/\text{s}$ or $100 \text{ \AA}^2/\text{ns}$ for all samples, qualitatively representative of the average diffusion constant of cations and anions of light alkali-halide (NaCl, KCl) salts in water.

M	Λ/d_{++}	$\langle \xi \rangle$	$D_{MC} [d_{++}^2/\tau]$	$\delta t/\tau$ [ns / MC step]
2	10	0.20 ± 0.02	1.60 ± 0.05	0.28 ± 0.01
1	10	0.36 ± 0.04	2.89 ± 0.04	0.52 ± 0.02
0.5	10	0.50 ± 0.03	3.97 ± 0.04	0.71 ± 0.01
0.1	10	0.72 ± 0.03	5.80 ± 0.05	1.04 ± 0.03
0.01	10	0.90 ± 0.04	7.30 ± 0.05	1.31 ± 0.02
2	19.4	0.18 ± 0.03	5.56 ± 0.08	1.005 ± 0.02
1	14.2	0.34 ± 0.04	5.56 ± 0.06	1.004 ± 0.02
0.5	11.9	0.49 ± 0.04	5.54 ± 0.08	0.996 ± 0.02
0.1	9.8	0.72 ± 0.02	5.55 ± 0.05	1.003 ± 0.01
0.01	8.6	0.90 ± 0.03	5.58 ± 0.07	1.008 ± 0.02

The electrostatic potential difference across the interfacial double layer may affect the electron transfer rate in a variety of ways, some of which are covered by the model, and other that are instead excluded at this stage, although they might be added by model refinements. First of all, $\langle \varphi(R_e) - \varphi(0) \rangle$ is directly related to the charge density profile and, in particular, to its value at contact, as can be seen in Tab. II. Moreover, the electrostatic potential contributes to the electrochemical potential $\bar{\mu} = \mu + \varphi$ for the ions but also for the electrons, thus shifting the energy of filled and empty states centred on the ions, and affecting their alinement with the corresponding levels on the electrode side. This effect, not included in the present model, could affect the charge transfer especially in the case of transition metal electrodes, which, because

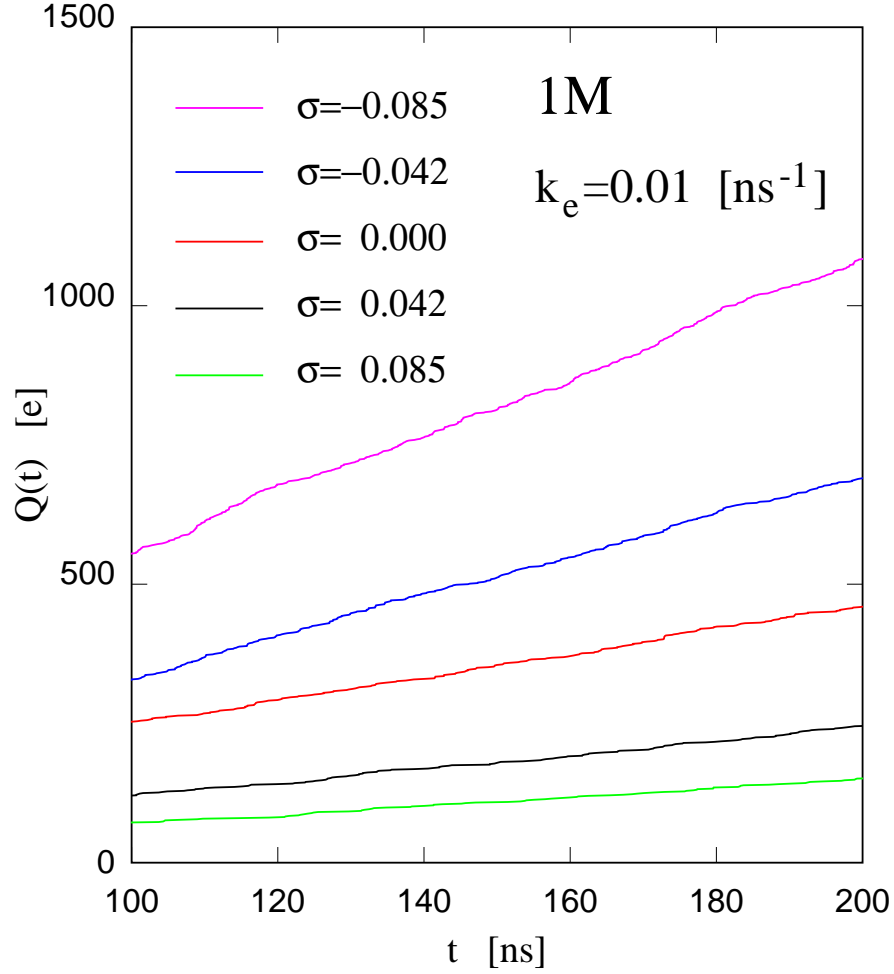


FIG. 5: Number of electrons transferred from the electrode to the cations as a function of time, across an interface of $9460 d_{++}^2$ area. Simulation carried out on a sample consisting of about 8000 ions at 1M concentration. To show that the flow of charge is fluctuating, a short portion (100 ns after the 100 ns equilibration of the flow) of the trajectories has been selected, out of runs covering about $2.5 \mu s$ each. The rate of electron transfer per active ion is

$$k_e = 1 \times 10^{-2} \text{ ns}^{-1}.$$

of narrow d-bands, might show large variations of the electronic density of states over a small energy change. The modulation and fluctuations of the potential and electric field close to the

interface might have a more subtle effect, since they might change the activation barrier for the electron transfer from the electrode to the ions, significantly amplifying or quenching the rate of the process. These effects can be modelled and their quantitative importance can be investigated by simulation. At this validation stage, however, they have been neglected, also because tuning the model and estimating the electron transfer parameters from the electronic structure requires a more detailed and quantitative picture of the system.

A further quantity relevant for the interpretation of the results for the electron transfer simulation is the differential capacitance of the interface C_D , defined as:

$$C_D(\sigma) = \frac{\partial Q}{\partial \phi_d}(\sigma) \quad (19)$$

C_D has been determined by fitting the σ dependence of the $\langle \varphi(R_e) - \varphi(0) \rangle$ values collected in Tab. II and then differentiating the fit. The results for $C_D(\sigma = 0)$ are also given in Tab. II. In the present context, the determination of C_D is important because knowing the differential capacitance of the interface allows to establish a one-to-one relation between surface charge and potential at the electrode. This, in turn, provides a way to translate the results obtained under charge control condition to the voltage control condition that directly corresponds to the experiments.

B. Calibration of the diffusion kinetics of ions

To set the stage for the electron transfer simulations, the diffusion of ions in MC time has been computed for samples of the same $M=0.01; 0.10; 0.5; 1; 2$ molar concentrations as in the previous subsections. Ideally, one is looking for the relation between the MC and real time diffusion for a given force field model (i.e., the primitive model of electrolyte solutions), independently from the the specific application and unaffected by the presence of the interface and by its curvature. For this reason, this computation has been carried out on homogeneous samples consisting of 4000 neutral ion pairs in a cubic simulation box with periodic boundary conditions applied. To avoid the complication of dealing with the discontinuous change in the number and identity of particles implied by the GCMC approach, this part of the simulations has been carried out using the canonical ensemble MC, excluding the grand canonical moves. The volume is fixed at the value corresponding to 4000 ion pairs at the target molarity.

For the sake of computational convenience, during this preliminary investigation of ionic

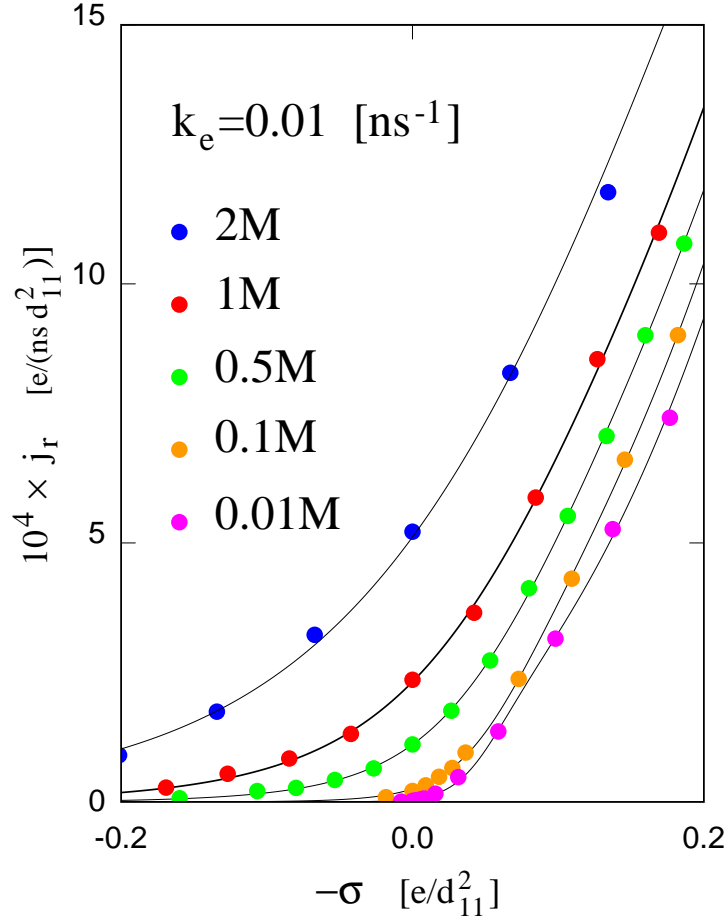


FIG. 6: Modulus j_r of the radial component of the current density \mathbf{j} across the metal / electrolyte interface as a function of the surface charge density σ and molarity M . Dots: simulation results. Full line: interpolations by the function in Eq. 20.

diffusion, the potential energy has been computed using the minimum image convention (mic), which is the standard choice with short range interactions, while long range potentials, like the Coulombic one, in extended periodic systems are routinely dealt with using Ewald summation methods. The choice of mic, which, incidentally, is the same as the one of Refs. 11,14, is partly justified by the fact that the side L of each sample is at least ten times longer than the screening length, qualitatively estimated by the Debye-Hückel length λ_{DH} , reported in

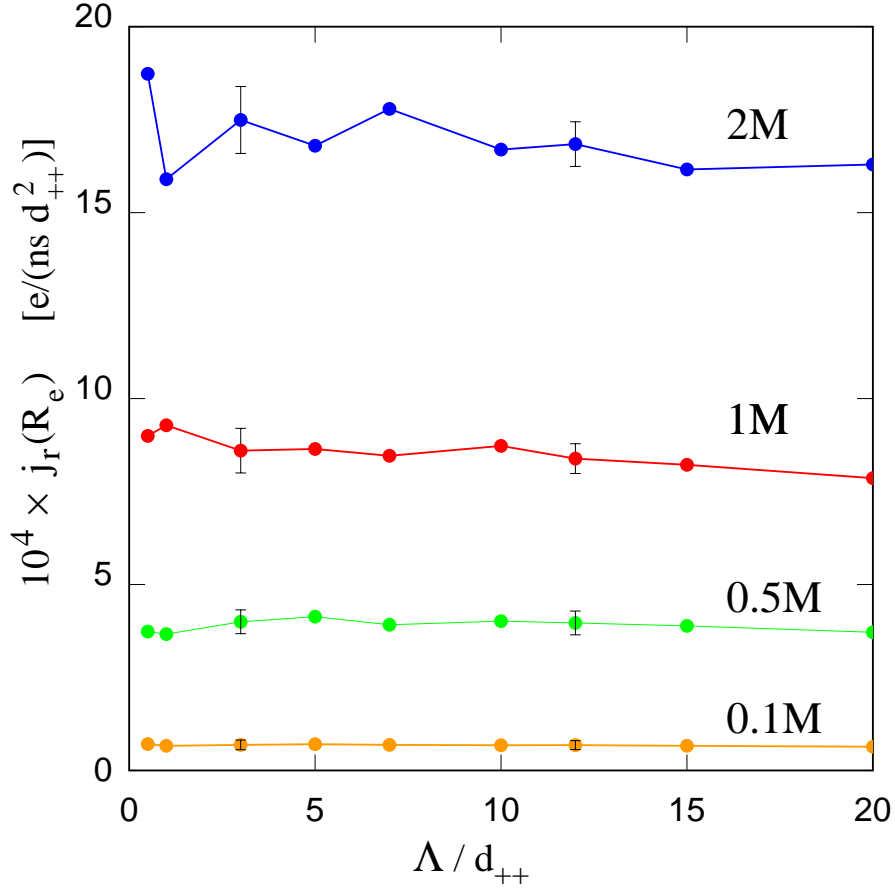


FIG. 7: Radial current density $j_r(R_e)$ through the electrode/electrolyte solution interface for all the simulated samples as a function of the amplitude Λ of the attempted MC displacement of single ions. For each choice of Λ and molar concentration M , the time scale of the simulation has been gauged according to the protocol described in Sec. III B, starting from the computation of the diffusion coefficient D_{MC} in MC time. Representative error bars are reported.

Tab. I. A (slight) exception to this $L/\lambda_{DH} > 10$ rule has to be noted only for the most dilute sample (0.01M concentration), for which screening is particularly ineffective. Moreover, diffusion properties are more sensitive to the short range part of the interparticle potential than to its long range tail, which, instead, might be more important for the thermodynamic

properties of the simulated samples. Remarkably, we observe that, at equal number of particles, i.e., 4000 ion pairs, the same value of mean activity coefficient γ_{\pm} that gives the target molarity in the neutral and charged spherical samples, results in the same molarity for the cubic boxes simulated under the mic boundary condition. This close correspondence suggests that even the thermodynamic properties, which are likely to be the most affected by the boundary conditions, are not significantly spoiled by the error due to the minimum image convention.

The results for the diffusion coefficient D_{MC} are reported in Tab. IV for the samples of molarity $0.01 \leq M \leq 2$. As already said, D_{MC} depends significantly on the step size Λ for the attempted displacement moves. Two values of Λ have been considered: i) $\Lambda = 10d_{++}$, which achieves an acceptance ratio of $0.2 \leq \xi \leq 0.6$ for $0.01 \leq M \leq 2$, and, ii) for each molarity, the Λ such that $D_{MC} = D$, for which a MC sweep over all particles correspond to 1 ns in real time. These two choices illustrate the fact that one could choose the MC step *a priori*, using the computed $\delta t/\delta \tau$ to translate MC time in real time units, or, for each concentration of the electrolyte, one could figure out what is the MC step that provides a given fixed value of the time conversion ratio. The first choice, i.e., a fixed $\Lambda = 10d_{++}$. is the one used for the simulations whose results are presented below. It turns out that there is no unique choice for Λ and the two sets of values given in Tab. IV are only representative of a whole range of acceptable values. We verified that a broad choice of Λ can be combined with the corresponding value of $\delta t/\delta \tau$ to give a virtually equivalent description of the flow of electrons through the interface. Quantitative support to this statement is given in Sec. III C below. It is likely that this freedom in selecting Λ is enjoyed only by models of dilute systems, whose MC sampling of the phase space is weakly dependent on the choice of the MC step. Denser samples might offer a much narrower choice for the Λ and D_{MC} , limited by low acceptance ratio for large Λ or prohibitively slow diffusion in MC time for short Λ .

To give an idea of the advantage of this kinetic interpretation of MC enjoys with respect to molecular dynamics, let us consider the choice of Λ such that $D_{MC} = D$ reported in Tab. IV. This choice implies that a sweep over particles, covers 1 ns. This is achieved with step amplitudes that provide an acceptance ratio well in excess of $\xi = 0.1$, which often is considered the minimum MC standard. Moreover, since energies are updated and not recomputed after each attempted move, the computational cost of one full sweep over ions is comparable to a single computation of the potential energy from scratch. Then, taking into account that usual MD time steps are of the order of the fs, it is easy to realise that the efficiency advantage of MC

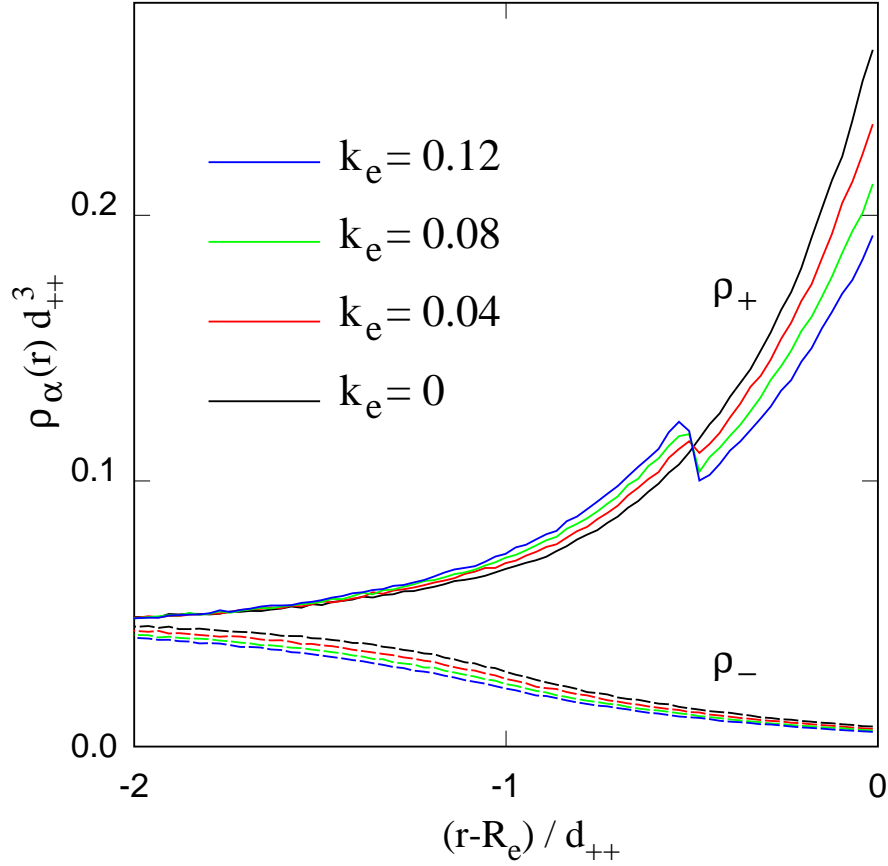


FIG. 8: Dependence of the density profiles of cations (ρ_+ : full lines) and anions (ρ_- : dash lines) on the rate of electron transfer per active atom. The discontinuities in $\rho_+(r)$ mark the boundaries of the active layer at $r = (R_e - \delta R)$ and $r = R_e$, with $\delta R = d_{++}/2$. The anion density profile ρ_- is continuous with a slight discontinuity in its derivative which cannot be appreciated on the scale of the figure.

over MD is of the order of five to six orders of magnitude. To a large extent, this excellent performance of MC is due to the dilute state of the samples, that allows MC steps of (nearly) arbitrary length with non-vanishing acceptance probability. Although it certainly cannot be generalised, a large advantage of the MC time evolution over the MD one is likely to be enjoyed over a broader range of models and simulation conditions than explored in the present study.

C. Electron transfer simulations

The MC simulations of the spherical samples have been extended to include the moves that represent the electron transfer from the electrode to the active cations, i.e., those within the thin active layer of width $\delta R = d_{++}/2$ at the interface. Two series of simulations have been carried out. In one case, attempted displacement and electron transfer moves are accompanied by grand-canonical moves that sample different numbers of ions in the system. Attempted displacement and grand canonical moves alternate each other at random, with the latter being tried, on average, every 10^3 attempted displacement ones. Simulations belonging to the second sequence exclude the purely grand canonical moves, and include only attempted displacements and electron transfer events. In all cases, the electron transfer occurs at a time selected from the exponential probability distribution as explained in Sec. II. Including grand canonical moves, even at low rate, has the advantage that the simulated system is in equilibrium with a known bulk state, defined by its excess chemical potential. Excluding these moves, instead, has the advantage of making more precise the relation between diffusion and time that underlies the approach being proposed. It turns out that all aspects of the simulated systems provided by the two algorithms are indistinguishable from each other. In what follows all data and plots are from the simulations without the grand canonical moves.

Following the protocol outlined in Sec. II, simulations start from a configuration well equilibrated by the GCMC method. All active ions are identified and given an expiration time, whose common origin is the system time $t_s = 0$. After this initial time, the synchronisation of the ion lifetimes is quickly lost, with some active ions being neutralised, and new ones joining the active class at virtually random times. The beginning of the simulation, when the aging of active ions is synchronised and the density profile of the ions at the interface has not been affected yet by the flow of charge, might differ from the stationary state of charge transfer and diffusion of ions through the system, when ions become active (by their random translation) and undergo neutralisation at uncorrelated times. To prevent biasing the results, a transient stage of about 100 ns is discarded from the time dependent simulation before starting to accumulate statistics. The transfer of electrons to the electrolyte cations, which is the subject of the investigation, is enhanced when the fluid side is positively charged and the surface charge is negative. For this reason, a few figures discussed in this section and in SI report properties as a function of $-\sigma$ instead of σ .

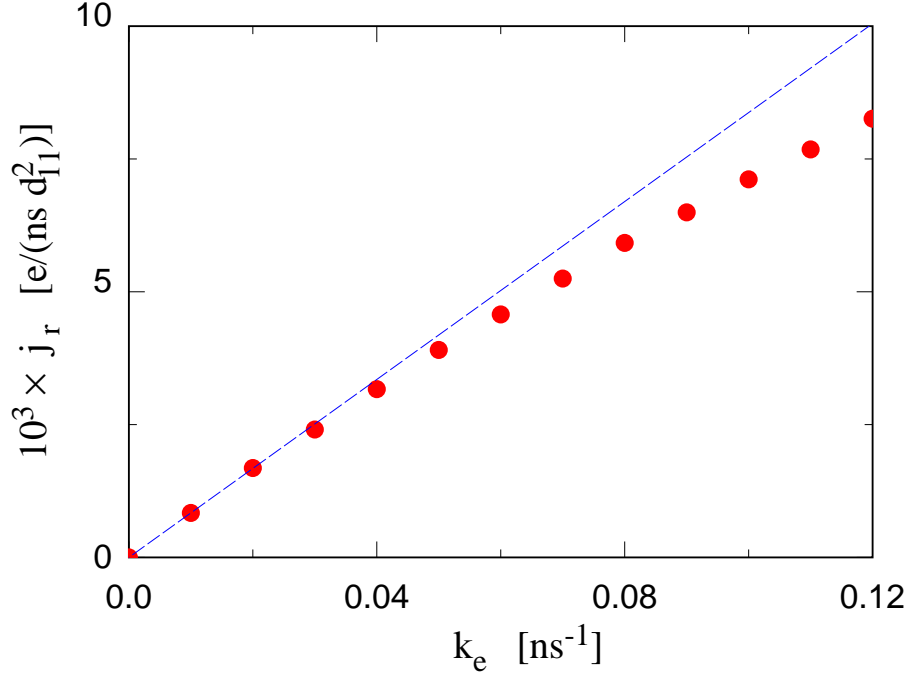


FIG. 9: Dependence of the radial current density $j_r(R_e|k_e)$ through the interface as a function of the kinetic coefficient k_e . The straight line is the tangent to $j(R_e|k_e)$ at the origin, and has been drawn to highlight the non-linearity of the simulation data.

The first quantity that we plot is the integral over time of the charge transferred from the electrode to the cations, that is shown in Fig. 5 as a function of time for different values of the surface charge density. The electrolyte concentration in the sample is 1M, and the rate of electron transfer per active ion is fixed in all cases at $k_e = 1 \times 10^{-2} \text{ ns}^{-1}$. Similar simulations have also been performed for all the other samples considered in this study, whose molarity goes from 0.01M to 2M.

The overall electron transfer rate per unit area at the interface, which represents a radial current density $\langle j_r(R_e) \rangle$, is obtained as the time derivative of the electron charge $Q(t)$ transferred per unit area. On average, the tangential components ($j_\theta; j_\phi$) of $\langle \mathbf{j} \rangle$ vanish by symmetry. The simulation results collected in Fig. 6 show the dependence of $\langle j_r \rangle$ on the surface charge σ for all

the samples of different electrolyte concentration. The strong dependence of $\langle j_r \rangle$ on negative values of σ reflects primarily the similar dependence on σ of the average surface density of active ions $\langle n_A \rangle$. This close relationship is highlighted by Fig. 7 in Sec. S5 of SI, plotting $\langle n_A \rangle$ as a function of σ for different molarities of the electrolyte, whose similarity with Fig. 6 is apparent. In turn, the dependence of $\langle j_r \rangle$ on $\langle n_A \rangle$, which, according to Eq. 15 grows quadratically with increasing $-\sigma$ values, suggests to fit both quantities with the functional form:

$$f(\sigma) = A(1 + \sigma^2) \frac{\exp(B\sigma)}{1 + C \exp(B\sigma)} \quad (20)$$

where $f(\sigma)$ is either $\langle j_r \rangle$ or $\langle n_A \rangle$, and A , B and C are the fit variables. This expression joins the quadratic growth of $f(\sigma)$ at large $-\sigma$ with a slow exponential-type decrease at large positive σ , when the electrostatic repulsion depletes the active layer of reactive ions. The fit is remarkably good, and, it has been verified that the overall scale parameter A depends very sensitively on the molarity of the solution and on the electron transfer rate k_e . The parameters B and C reflect primarily the screening properties of the electrolyte close to the interface. Notice that $\sigma = 0$, corresponding to the potential of zero charge (PZC) for the electrode, does not imply zero current, whose flow is dictated by the electron energy diagram in Fig. 1.

The $\langle j_r(\sigma) \rangle$ curves for the different electrolyte concentrations shown in Fig. 6 trivially converge to the zero current condition for large σ values, because of the vanishing of $\langle n_A \rangle$ in the same limit. More interestingly, the $\langle j_r(\sigma) \rangle$ curves seem to converge to a unique limiting curve also in the opposite limit of large $-\sigma$ values, in which the average surface density of active ions $\langle n_A \rangle$ becomes uniquely determined by σ^2 , as apparent from the relation in Eq. 15, at the same time as its dependence on the bulk osmotic pressure becomes negligible.

It is important to emphasise that the precise choice of the MC step Λ is not crucial to provide the correct description of the electron transfer kinetics, at least over a broad interval of values, and *provided* the conversion of MC time to real time is carried out according to the approach described in Sec. II and IIIB. To verify this important point, simulations have been carried out for all electrolyte concentrations already considered, varying the MC step Λ and converting time with the Λ and concentration dependent factor $\delta t/\tau$ that has been computed using the protocol specified in Sec. IIIB. The results, shown in Fig. 7, confirm that the choice of Λ is not unique, and produces equivalent results provided the set of (Molarity, Λ and $\delta t/\tau$) values are consistent. This feature allows to select Λ in such a way to optimally balance the efficiency (requesting wide Λ and long $\delta t/\tau$) as well as the time resolution (requesting narrow Λ and

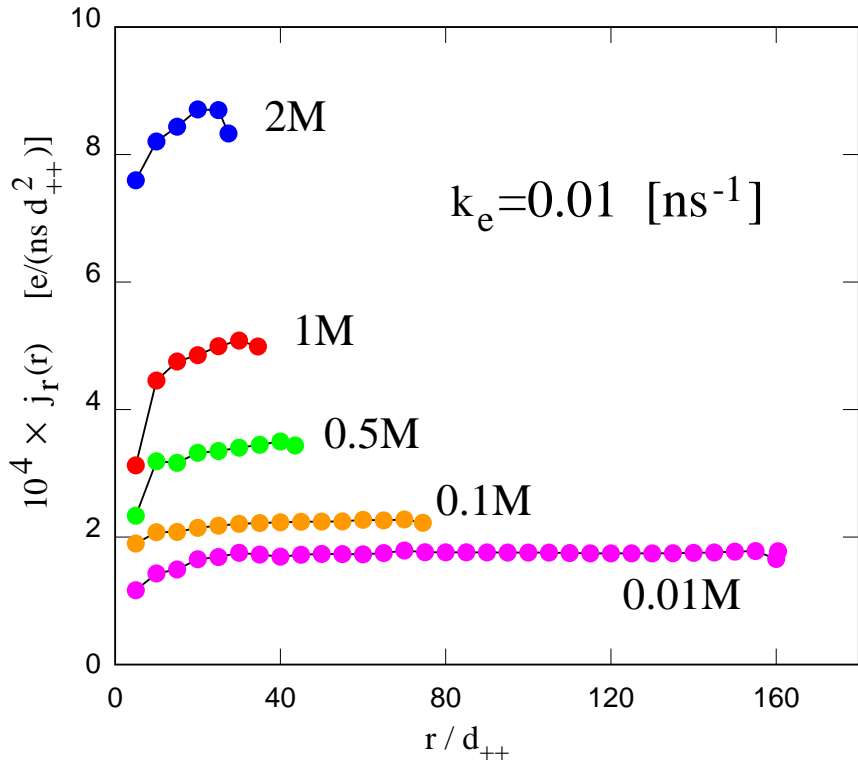


FIG. 10: Dependence of the radial component $j_r(r)$ of the current on the distance r from the centre of the spherical electrode (dots). The black full line is a guide to the eye. The last point of each curve corresponds to the electrode/electrolyte solution interface. While at the interface the charge flow is due to electrons neutralising cations, in the rest of the sample there is an ionic current of cations drifting towards the cathode.

short $\delta t/\tau$) of the MC evolution of the system. As already stated, there is no guarantee that this broad freedom in choosing Λ is shared by more realistic models of electrode/electrolyte interfaces, but even a narrower choice is likely to be compatible with the simulation study of a sizeable class of systems and models.

As repeatedly pointed out, the dependence of $\langle j(R_e) \rangle \equiv j_r(R_e)$ on σ is due primarily to the dependence of the contact density, and therefore of the number of active ions, on σ . An

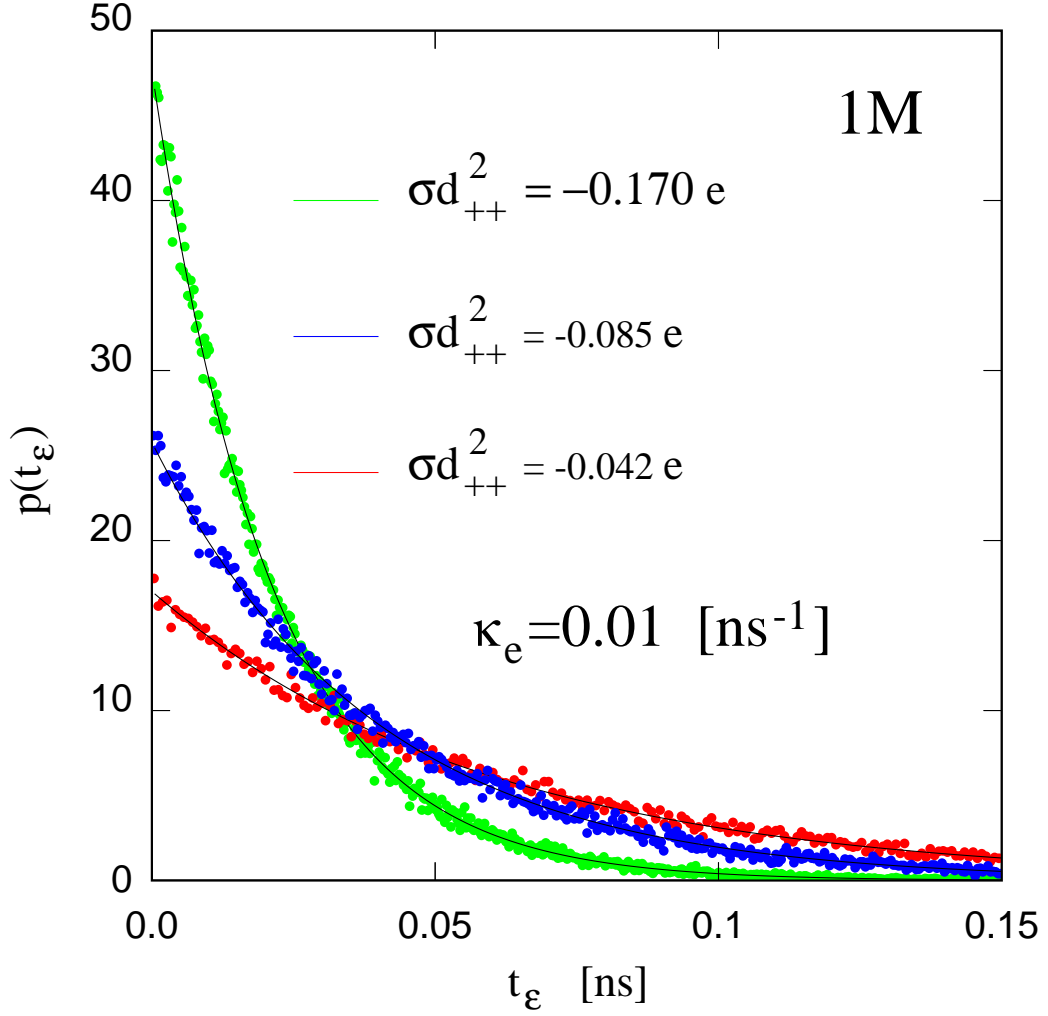


FIG. 11: Probability distribution for the time separation t_ϵ between successive electron transfer events. Sample of (nominal) 8000 ions at 1M concentration. The small dots in colours represent the simulation results. The full lines (black) correspond to the analytical result expressed by Eq. 22 with $\langle n_A \rangle$ computed by simulation for the three samples of different surface charge density σ .

additional dependence might come from the fact that the number of active ions depends on the current density $\langle \mathbf{j} \rangle$ itself, which tends to deplete the ion density at contact with the electrode.

This negative feedback mechanism is unambiguously confirmed by the simulation results. To emphasise this effect, charge transfer simulations have been carried out for systems whose surface charge density $-\sigma$ is large, exploring a range of k_e also extending up to fairly large values. The results are shown in Fig. 8. It is apparent that with increasing rate k_e , the density of cations in the active layer is increasingly depleted, while the density of anions in the same range is nearly unchanged. Just outside the active layer, i.e., for $r \leq R_e - \delta R$, the cation density is slightly enhanced, since the screening of the interfacial charge is less effective when the electron current is flowing. As a consequence of this depletion, the dependence of overall transfer rate \mathbf{j} on the k_e rate constant is slightly sub-linear, as shown in Fig. 9.

The choice of re-inserting the charge of the neutralised ions at a random position in the system volume according to the probability distribution $p_r(r)$ in Eq. 12 aims at obtaining a radial component $j_r(\mathbf{r})$ of the current that is independent from position and matches the flow of charge at the electrode/electrolyte solution interface. This requirement has been verified by considering a sequence of spherical surfaces concentric with the sample whose radii are spaced by a regular distance of $5d_{++}$. Then, the number and direction of cations and anions crossing each surface during the simulation is recorded, and transformed into the radial current $j_r(r)$ which represents the net transfer of ions across each unit surface (d_{++}^2) during a unit of (real) time. The results of this analysis of trajectories is reported in Fig. 10. It is apparent that the requirement of uniform j_r across the system is satisfied fairly well. A non-negligible deviation only occurs close to the origin, due to the transformation of $p_r(r) = 1/r$ into $p(r) = 1/(1+r)$ introduced to avoid dealing with a distribution which is singular at the origin.

As already pointed out, achieving a (nearly) uniform radial current ($j_r(\mathbf{r}) = k$) implies a violation of the continuity equation. After a short transient, in fact, $\partial\rho_Q(\mathbf{r})/\partial t = 0$ everywhere, while $\nabla \cdot \mathbf{J}(\mathbf{r}) = 2k/r$, thus:

$$\nabla \cdot \mathbf{J}(\mathbf{r}) + \frac{\partial\rho_Q(\mathbf{r})}{\partial t} = 2k/r \neq 0 \quad (21)$$

In these expressions, $\rho_Q(\mathbf{r}) = e[\rho_+(\mathbf{r}) - \rho_-(\mathbf{r})]$, where e is the electron charge. The violation of the continuity equation, however, cannot be avoided for this kind of processes, in which the interface is a sink of (in this case) cations. Since the system evolves under stationary conditions, the sink of cations needs to be compensated by an equivalent source, that also violates the continuity equation, and that in the model is represented by the re-introduction of the cations neutralised at the interface. Then, requesting $j_r(r) = k$ is only a way to decide

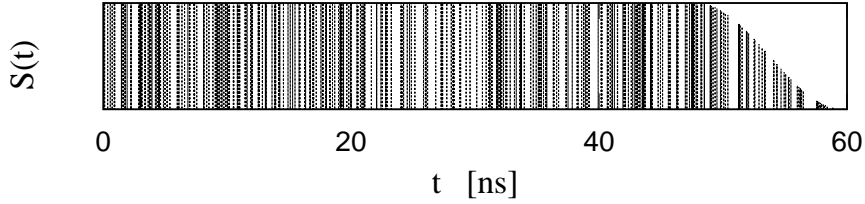


FIG. 12: Time series giving the exact time of each electron transfer in the sample of Fig. 5. The time series has been weighted by a windowing function equal to 1 up to 80 % of the total interval, and smoothly going to zero in the last 20 ns. For the sake of simplicity, the figure reports a time series much shorter than the one used to compute the power spectrum.

where and how strongly the violation affects the system. The other extreme choice would be to enforce the continuity equation *almost everywhere*, that however requires $j_r(\mathbf{r}) = k'/r^2$. In turn, this implies that the violation of the continuity equation is concentrated at the interface $r = R_e$ and at the origin $r = 0$. In this case, in addition, $j_r(\mathbf{r})$ is singular at the origin. Considering these two cases, we think that the $j_r(\mathbf{r}) = k$ choice is the least problematic one. In this respect, the planar case is somewhat easier, because in such a case the violation of the continuity equation can be confined at the two opposite interfaces.

Similarly to what has been found for structural and electrostatic properties, at equal charge density σ , the dependence of the current density on the size of the spherical sample is minor. Quantitative data are given in Sec. S6 of SI.

In the model of electron transfer described above, the rate constant k_e accounts for all contributions to the activation barrier that opposes the electron transfer itself. More refined models could be built by making the description of the barrier and of its different components more detailed. For instance, one could isolate the reorganisation energy from the other contributions, introducing a step-like potential that opposes the penetration of cations and anions into the active range. This simple addition would already give a more complex and richer model to simulate.

A crucial aspect of the proposed approach is that, at variance from the deterministic, continuous and delocalised picture of DFT-based approaches whose Kohn-Sham orbitals do not strictly correspond to real electrons, the model retains a discrete representation of both the electrons and their transfer across the interface. In particular, each electron transfer is a discrete event taking place at time t_i , whose sequential timing represents a time series $\{t_i, i = 1, \dots, \Pi\}$, whose statistics can be analysed in much detail.

The simplest analysis concerns the probability distribution of the separation t_ϵ between consecutive electron transfer events, shown in Fig. 11. Assuming, at first, that the time series is generated by a single active site, which remains unaltered by the transfer and continue to be active, the separation between successive events is precisely the random variable Δt whose distribution is given by Eq. 9. The probability distribution for the time separation of transfers taking place over the whole interface, however, is less predictable, since it results from the superposition of many exponential time series (as many as the number n_A of active ions), whose origin is not synchronised, and whose number is fluctuating in time. Nevertheless, the result conforms to the simplest possible guess: the average time separation is $\langle t_\epsilon \rangle = 1/(\langle n_A \rangle k_e)$ and the probability distribution is:

$$p(t_\epsilon) = \bar{K}_e \exp(-\bar{K}_e t_\epsilon) \quad (22)$$

with $\bar{K} = \langle n_A \rangle k_e$. This result is illustrated in Fig. 11.

A more refined statistical analysis could give insight into the relaxation processes that take place in the system, and also allow a connection with experimental observations. To carry out this analysis, the time series is written as:

$$\mathcal{J}(t) = \sum_{i=1}^{\Pi} y(t) \delta(t - t_i) \quad (23)$$

that represents the instantaneous current across the whole interface at time t . The function $y(t)$ is a suitable windowing function introduced to make Fourier-representable a sequence that otherwise is non-periodic. Its definition and application are illustrated in Fig. 12. The power spectrum, computed as the square of the Fourier transform of $\mathcal{J}(t)$, is shown on logarithmic scales in Fig. 13. Notice that the time series transformed to obtain the power spectrum is much longer than the one given in Fig. 12, being 30 μs long. The result is somewhat ambiguous, since Fig. 13 shows both a constant *white noise* background and a component which behaves like $1/f^\alpha$, with $1 \leq \alpha \leq 2$, the power spectrum contains aspects reminiscent of *flicker noise*.

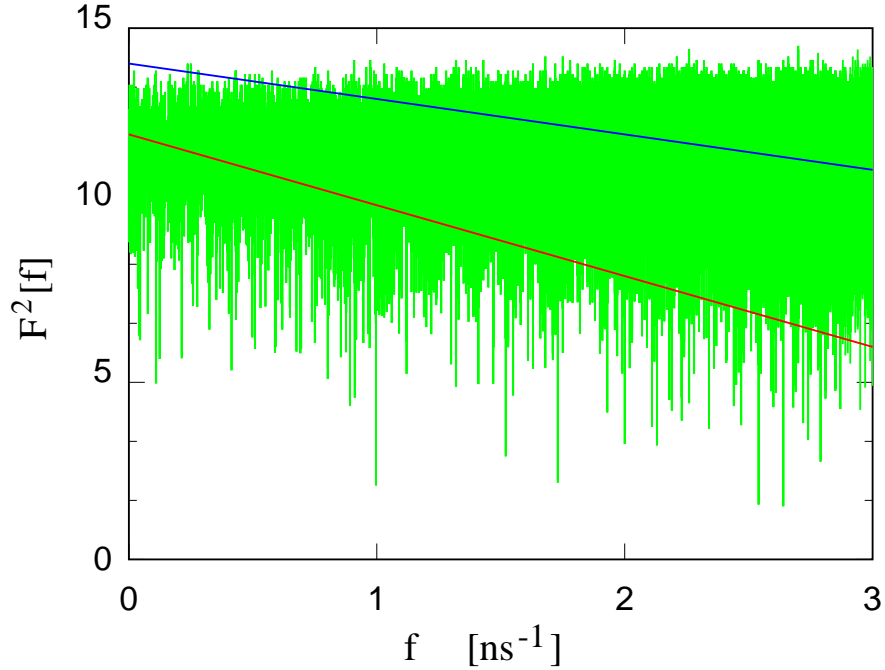


FIG. 13: Power spectrum (green line) of the time series giving the exact time of each electron transfer in the sample of Fig. 5. The power spectrum is computed as the square of the Fourier transform of the time series. Red line: line of slope $m = -2$. Blue line: line of slope $m = -1$.

These observations are highlighted by the two straight lines of slope -1 and -2 superimposed to the noise power spectrum in Fig. 13.

The second qualifying aspect of our model is its explicit coupling of the two processes that dominate the charge transfer at the electrode / electrolyte interface. To illustrate this dependence, the calibration of the correspondence between MC and real time has been repeated assuming that the ions diffuse in a solvent whose viscosity η_{sol} varies from 10% of the water value η_{H_2O} to $2000 \times \eta_{H_2O}$. This seemingly wide range is in fact rather moderate, considering that the viscosity of honey, for instance, is already $\sim 40 \times 10^3 \eta_{H_2O}$. The calibration has been carried out by scaling the diffusion constant of the ions using the Stokes-Einstein relation ($D \times \eta = constant$), which, although not quantitatively accurate, reproduces the correct trend

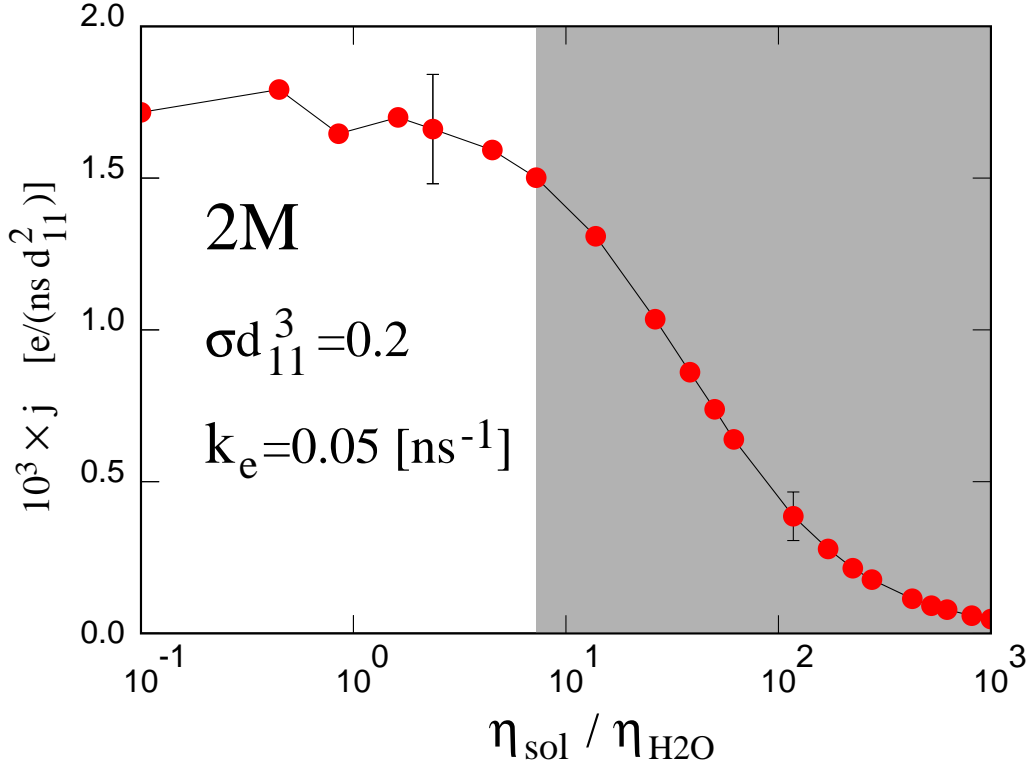


FIG. 14: Radial component j_r of the current density across the electrode / electrolyte solution interface as a function of the viscosity η_{sol} of the solvent in which the electrolyte ions diffuse. Representative error bars are given. The viscosity is measured in units of the water viscosity coefficient η_{H_2O} . The calibration of the real time t to MC time τ conversion relies on the Stokes-Einstein relation to estimate the real-time diffusion coefficient of the ions in the solvent of any given viscosity, starting from the $D = 10^{-5}$ cm²/s value adopted for their diffusion in water at standard conditions, irrespective of concentration in the $0.01 \leq M \leq 2$) range. Dots: simulation results. The full line is a guide to the eye. The gray area identifies the $\eta_{sol}/\eta_{H_2O} \geq 10$ range in which the electron transfer is limited by diffusion.

and order of magnitude for the relatively dilute solutions of the present study. Then, simulations have been carried out for solutions of 2M concentrations, with the surface charge density $\sigma = 0.2$ e/d₊₊², and electron transfer rate $k_e = 0.05$ ns⁻¹. In each case the MC step Λ for the attempted

displacement of the ions was fixed at $10d_{++}$, and the time conversion factor was selected as specified in the previous sentences of this paragraph. The results of these simulations are reported in Fig. 14. It is apparent that increasing η_{sol} , thus decreasing the diffusion rate in real time, enhances the depletion of the active layer of reactive ions, and decreases the overall electron transfer rate. For $\eta_{sol} > 10\eta_{H_2O}$ (corresponding to the gray area in Fig. 14), the electron transfer rate is diffusion limited, while below this value of η_{sol} the process is limited by the kinetic parameter k_e . The transition between the two regimes is relatively sharp.

IV. SUMMARY AND CONCLUSIONS

Simulating the electron transfer at electrochemical interfaces is a crucial goal which could greatly impact multiple conceptual and applied research topics. The process encompasses a number of electronic structure aspects, concerning the energy spectrum and spatial localisation of filled and empty states on the two sides of the interface, as well as statistical mechanics aspects, concerning the distribution of ions in the diffuse layer at the interface and the strength and fluctuations of the electrostatic potential (and corresponding electric field) on the electrolyte solution side. Kinetics is also very important, both for the electron transfer process, controlled by activation barriers and affected by quantum and thermal fluctuations, and also for the diffusion of ions in solution, which is required for reaching a stationary state during the operation of the electrochemical device to which the electrode / electrolyte interface belongs. The electron transfer involves only the active ions in the immediate vicinity (order of the Å) of the electrode, while diffusion involves all the electrolyte ions, whose precise state can be fixed by applying the GCMC algorithm, which provides the required connection with an extended reservoir of known thermodynamic conditions.

Seen from the time scale of diffusive and relaxation processes in the electrolyte solution, the electron transfer is a sudden event taking place after a long lag time whose random duration reflects the probabilistic nature of quantum mechanical events. These aspects orient the choice of the overall simulation method to Monte Carlo, able to deal with discontinuous and stochastic aspects, and also to bypass the high frequency vibrational aspects that limit the time span of atomistic molecular dynamics simulations, retaining diffusion and the relaxation processes that drive the long term evolution of the system. Diffusion, in particular, couples the stochastic electron jumps and the atomistic processes that involve the electrolyte ions. After a relatively

short transient, the mean square displacement of the ions depends linearly on time in real-life diffusion. In a similar way, the mean square displacement of the ions depends linearly on the number of steps in MC, which represents the closest analogue to an intrinsic time scale in MC simulations. In the present approach, the rate of the two processes are connected by imposing that real and MC time are equivalent when they result in the same increase of mean square displacements. This gives a way to express the MC evolution in real time units and to synchronise diffusion and electron transfer in the model. The model and the simulation protocol introduced in Sec. II reflect all these aspects, although, to highlight the most important features unencumbered by details, it does it in the simplest possible way. Arguably one of the most crude simplification is the fact that the electrolytic solution is described at the implicit solvent level. Together with the moderate electrolyte concentration (up to 2M), the implicit solvent assumption allows to reposition ions from the interfacial active layer to well inside the spherical sample, as required to simulate the kinetics of cations' neutralisation by the transferred electrons while: (i) conserving the total sample charge; (ii) sustaining the same radial current density throughout the system, from an inner spherical core up to the interface.

Monte Carlo simulations of the coupled electron transfer and ionic diffusion carried out by the model of Sec. II show that, after a relatively short transient, the samples reach a stationary state in which the depletion of active ions is compensated by diffusion. The interplay, and, in some instances, the competition between these two mechanisms determines a range of features concerning the steady state operation of the electrochemical interface. For instance, depending on the electrolyte solution viscosity, the process presents two regimes (see Fig. 14), the first one being diffusion limited, the second one being limited by the inherent electron transfer rate per active ion k_e . Of course, the diffusion limited regime corresponds to low values of the ions' diffusion constant, the second one corresponds to high values of D and D_{MC} , and the transition between the two regimes is fairly sharp. Moreover, the partial replenishment of the depleted active ions results in the sub-linear dependence of the overall transfer rate on the kinetic coefficient k_e .

The implemented model is particularly simple, since it corresponds to the scheme of Fig. 1, and neglects the feedback on the electronic levels due to the value and the fluctuations of the electrostatic potential driven by the interfacial charge and electron flow. In this simplified picture, the primary reason for the dependence of the overall transition rate on the electrode surface charge density σ is represented by the similar dependence of the number of active ions

on the surface charge. The resulting $j_r(\sigma)$ function is modelled by the fit in Eq. 20, and, at large $-\sigma$ values, primarily reflects the contact density theorem expressed by Eq. 15.

The correspondence between the stochastic evolution of the model and real time provides an opportunity to investigate the size and nature of the noise in the current flow. The model, however, is likely to be still too sketchy to provide a reliable account of this complex property. Results from the present simulations, plotted in Fig. 13, give an uncertain answer, showing aspects that could suggest both a white or a flicker noise signature. Better models, including feedback of the electrostatic potential strength and fluctuations on filled and empty electronic states on the ions might change the picture and provide a more definite result.

Besides adding the effect of electrostatics on the (empty and filled) electron energies of ions, many other opportunities exist to improve the model, covering a wider range of phenomena and making the approach more predictive. For instance, the further role of the ion whose oxidation state is being changed at the interface is left unspecified by the present model. However, the model could be extended by attributing realistic interactions to the transformed species, opening the way to a more comprehensive description of electrochemical devices, up to the complexity of Galvanic and fuel cells. Moreover, the model neglects the effect of the electric field at the interface on the reaction barrier that determines k_e . This effect, however, could be modelled and reintroduced, opening the way to verify by simulation the validity and microscopic origin of Volmer-Butler equation.² A first step in modeling k_e and its dependence on various contributions could consist in isolating the effect of the reorganisation energy from other, more genuinely electronic factors. The reorganisation energy, in particular, could be mimicked by a repulsive step potential that could limit the access of ions to the active layer.

The description of the electronic part of the process could be improved by adding an atomic-like quantum Hamiltonian to the active ions, with an explicit coupling with the electron states spilling out of the electrode. This extension is certainly ambitious and challenging, but it would open the way to semi-quantitatively including non-adiabatic effects into the electron kinetics at the interface.³¹

One of the aspects that most urgently requires improvements is the need to carry out random, long distance displacements of ions from the active layer to well inside the electrolyte solution side of the interface, as described at the end of Sec. II. In practice, this can be carried out only at low fluid particles density, but it would hardly be feasible with a dense, explicit solvent model. Removing this limitation is challenging, but recent developments (involving the adaptive

resolution algorithm³²⁻³⁵) might indicate the way forward. In this method, the portion of the system described in atomistic detail is coupled with an ideal gas reservoir of known chemical potential, in which the insertion, removal or long range random displacement of particles can take place with virtually unit probability. These features could be slightly adapted to produce a gradient of electrochemical potential, which, in turn, would force a stationary flow of current similar to what has been obtained in the present case.

Even before these improvements and extensions will be made, the present scheme and its implementation represent a rich statistical mechanics model to investigate open systems operating at steady state conditions, mixing quantum and classical aspects in their time evolution, whose detailed analysis could shed light on many complex aspects of electrochemical interfaces.

ACKNOWLEDGMENTS: D.V.-D., F. S. and N.C.F.-M. acknowledge the Deutsche Forschungsgemeinschaft (DFG, German Research Foundation) for funding through the research group FOR 2982–UNODE, Project number 413163866. N.C.F.-M. gratefully acknowledges the ECHELON Project from the Carl Zeiss Foundation for financial support. R.C.-H. acknowledges the European Union for funding through the Twinning project FORGREENSOFT (grant no. 101078989 under HORIZON-WIDERA-2021-ACCESS-03). R.C.-H. and F.S. acknowledge funding from SFB-TRR146 of the German Research Foundation (DFG)–Project No. 233630050. One of us (PB) thanks Andrea Grisafi for useful discussions.

-
- ¹ Marek Nowicki, Klaus Wandelt, Metal-Electrolyte Interfaces. In *Surface and Interface Science*, K. Wandelt (Ed.). <https://doi.org/10.1002/9783527680603.ch57>.
 - ² The Electrified Interface. In *Modern Electrochemistry 2A: Fundamentals of Electrodics*; Bockris, J. O. M., Reddy, A. K. N., Gamboa-Aldeco, M., Eds.; Springer US: Boston, MA, 2000; pp 771-1033.
 - ³ Atkins, P. W.; de Paula, J.; Keeler, J. J. *Atkins' Physical Chemistry*, eleventh ed.; Oxford University Press: Oxford, New York, 2018.
 - ⁴ Marcus, R. A. On the theory of oxidation-reduction reactions involving electron transfer, *I. J. Chem. Phys.* **1956**, *24*, 966-978.
 - ⁵ Marcus, R. A. On the theory of electron-transfer reactions. VI. Unified treatment for homogeneous and electrode reactions. *J. Chem. Phys.* **1965**, *43*, 679-701.
 - ⁶ Hush, N. S. Adiabatic rate processes at electrode 1. Energy-charge relationships. *J. Chem. Phys.*

- 1958**, *28*, 962-972.
- ⁷ Santos, E.; Schmicker, W. Models of electron transfer at different electrode materials. *Chem. Rev.* **2022** *122*, 10581-10598.
- ⁸ Price, D. L.; Halley, J. W. Molecular dynamics, density functional theory of the metal–electrolyte interface. *J. Chem. Phys.* **1995**, *102*, 6603-6611.
- ⁹ Trasatti, S., Lust, E. (2002). The Potential of Zero Charge. In: White, R.E., Bockris, J.O., Conway, B.E. (eds) Modern Aspects of Electrochemistry. Modern Aspects of Electrochemistry, vol 33. Springer, Boston, MA.
- ¹⁰ Dufrêche, J. F.; Bernard, O.; Turq, P.; Mukherjee, A.; Bagchi, B. Ionic self-diffusion in concentrated aqueous electrolyte solutions. *Phys. Rev. Lett.* **2002**, *88*, 095902.
- ¹¹ Valleau, J. P.; Cohen, L. K. Primitive model electrolytes. I. Grand canonical Monte Carlo computations. *J. Chem. Phys.* **1980**, *72*, 5935-5941.
- ¹² Beeler, J. R., Jr. Displacement Spikes in Cubic Metals. I. α -Iron, Copper, and Tungsten. *Phys. Rev.* **1966**, *150*, 470-487.
- ¹³ Voter, A. F. in Radiation Effects in Solids, edited by K. E. Sickafus and E. A. Kotomin (Springer, NATO Publishing Unit, Dordrecht, The Netherlands, 2005).
- ¹⁴ Torrie, G. M.; Valleau, J. P. Electrical double layers. I. Monte Carlo study of a uniformly charged surface. *J. Chem. Phys.* **1980**, *73*, 5807-5816.
- ¹⁵ Modern Theoretical Chemistry 5. Statistical Mechanics, Part A: Equilibrium Techniques: Edited by B.J. Berne. Plenum Press, New York, 1977.
- ¹⁶ Quiñones, A. O.; Bhuiyan, L. B.; Outhwaite, C. W. Thermodynamics of primitive model electrolytes in the symmetric and modified Poisson-Boltzmann theories. A comparative study with Monte Carlo simulations. *Cond. Matter Phys.* **2018**, *21*, 23802.
- ¹⁷ Rigo, E.; Dong, Z.; Hyun Park, J.; Kennedy, E.; Hokmabadi, M.; Almonte-Garcia, L.; Ding, L.; Aluru, N.; Timp, G. Measurements of the size and correlations between ions using an electrolytic point contact. *Nature Commun.* **2019**, it 10, 2382.
- ¹⁸ Ballone, P.; Pastore, G.; Tosi, M. P.. *J. Chem. Phys.* **1986**, *85*, 2943-2950.
- ¹⁹ Giera, B.; Henson, N.; Kober, E. M; Shell, M. S.; Squires, T. M. Electric double-layer structure in primitive model electrolytes: Comparing molecular dynamics with local-density approximations. *Langmuir* **2015**, *31*, 3553-3562.
- ²⁰ Andersson, L.; Zhang, C. Molecular dynamics simulations of metal-electrolyte interfaces under

- potential control. *Curr. Opin. Electrochem.* **2023**, *42*, 101407.
- ²¹ Dwelle, K. A.; Willard, A. P. Constant potential, electrochemically active boundary conditions for electrochemical simulation. *J. Phys. Chem. C* **2019**, *123*, 24095-24103.
- ²² Feynman, R. P. *The Feynman Lectures on Physics, the New Millennium Ed.*; Basic Books: New York, NY, 2011; Vol. 2 Mainly Electromagnetism and Matter.
- ²³ J. C. Tully, in *Modern Theoretical Chemistry: Dynamics of Molecular Collisions*, edited by W. H. Miller (Plenum, New York, 1976), p. 217.
- ²⁴ Toldo, J. M.; do Casal, M. T.; Ventura, E.; do Monte, S. A.; Barbatti, M. Surface hopping modeling of charge and energy transfer in active environments. *Phys. Chem. Chem. Phys.* **2023**, *25*, 8293-8316.
- ²⁵ Anderson, P. W. Localized magnetic states in metals. *Phys. Rev.* **1961**, *124*, 41-53.
- ²⁶ Newns, D. M. Self-consistent model of hydrogen chemisorption. *Phys. Rev.* **1969**, *178*, 1123-1135.
- ²⁷ Cuppen, H. M.; Karssemeijer, L. J.; Lamberts, T. The kinetic Monte Carlo method as a way to solve the master equation for interstellar grain chemistry. *Chem. Rev.* **2013**, *113*, 8840-8871.
- ²⁸ Gillespie, D. T. Stochastic simulation of chemical kinetics. *Annu. Rev. Phys. Chem.* **2007**, *58*, 35-55.
- ²⁹ Henderson, D.; Blum, L.; Lebowitz, J. L. An exact formula for the contact value of the density profile of a system of charged hard spheres near a charged wall. *J. Electroanal. Chem.* **1979**, *102*, 315-319.
- ³⁰ Jackson, J. D. *Classical Electrodynamics*, 3rd ed.; John Wiley and Sons, 1999.
- ³¹ Schmickler, W.; Mohr, J. The rate of electrochemical electron-transfer reactions. *J. Chem. Phys.* **117**, 2867-2872 (2002).
- ³² Praprotnik, M.; Delle Site, L.; Kremer, K. Adaptive resolution molecular-dynamics simulation: Changing the degrees of freedom on the fly. *J. Chem. Phys.* **2005**, *123*, 224106.
- ³³ Potestio, R.; Fritsch, S.; Español, P.; Delgado-Buscalioni, R.; Kremer, K.; Everaers, R.; Donadio, D. Hamiltonian Adaptive Resolution Simulation for Molecular Liquids. *Phys. Rev. Lett.* **2013**, *110*, 108301.
- ³⁴ Baptista, L. A.; Dutta, R. C.; Sevilla, M.; Heidari, M.; Potestio, R.; Kremer, K.; Cortes-Huerto, R. Density-functional-theory approach to the Hamiltonian adaptive resolution simulation method. *J. Phys. Condens. Matter.* **2021**, *33*, 184003.
- ³⁵ Sevilla, M.; Baptista, L. A.; Kremer, K.; Cortes-Huerto, R. Density fluctuations, solvation ther-

modynamics, and coexistence curves in grand canonical molecular dynamics simulations. *J. Chem. Phys.* **2025**, *162*, 080901.